

**Study on Structural Performance of FRCC  
Beam-Column Joints using Discrete Polymer Fibers**

March 2020

MU YU

**Study on Structural Performance of FRCC  
Beam-Column Joints using Discrete Polymer Fibers**

Graduate School of Systems and Information Engineering

University of Tsukuba

March 2020

MU YU

# CONTENTS

LIST OF TABLES.....	III
LIST OF FIGURES.....	IV
DISSERTATION ABSTRACT.....	1
CHAPTER 1 Introduction.....	7
1.1 Research Background.....	7
1.2 Literature Review.....	9
1.3 Objective and Scope.....	12
1.4 Outline of the Thesis.....	14
CHAPTER 2 Tensile and Bending Behavior of FRCC.....	18
2.1 Introduction.....	18
2.2 Uniaxial Tension Test.....	19
2.2.1 Outline of experiment.....	19
2.2.2 Experimental results and discussion.....	22
2.3 Bending Test.....	31
2.3.1 Outline of experiment.....	31
2.3.2 Three-point bending test.....	31
2.3.3 Four-point bending test.....	33
2.4 Conclusions.....	35
CHAPTER 3 Influence of Fiber Types on Structural Performance of FRCC Beam-Column Joints.....	36
3.1 Introduction.....	36
3.2 Experimental Program.....	37
3.2.1 Specimens.....	37
3.2.2 Materials properties.....	40
3.2.3 Loading and measurement.....	42
3.2.4 Experimental results.....	44
3.3 Conclusions.....	52
CHAPTER 4 Influence of Casting Method on Structural Performance of FRCC Beam-Column Joints.....	53
4.1 Introduction.....	53
4.2 Experimental Program.....	54
4.2.1 Specimens and materials properties.....	54

4.2.2 Casting methods .....	55
4.2.3 Loading and measurement.....	57
4.2.4 Experimental results .....	57
4.3 Conclusions .....	59
CHAPTER 5 Evaluation of Shear Capacity of FRCC Beam-Column Joints .....	60
5.1 Introduction .....	60
5.2 Proposed Evaluation Method for FRCC Beam-Column Joint .....	60
5.3 Verification .....	63
5.4 Conclusions .....	64
Chapter 6 Conclusions .....	65
REFERENCES .....	67
ACKNOWLEDGEMENTS .....	72
PUBLICATIONS ARISING FROM THE THESIS .....	73

## LIST OF TABLES

Table 2. 1 Mechanical properties of fiber.....	19
Table 2. 2 Mixture proportion of FRCC.....	20
Table 2. 3 Mechanical properties of concrete.....	20
Table 2. 4 Tensile test results of specimens without notch.....	24
Table 2. 5 Counted total number of fiber across section of specimens without notch .....	26
Table 2. 6 Tensile test results specimens with notch .....	28
Table 2. 7 Counted total number of fibers across section of specimens with notch.....	30
Table 3. 1 Specimens list.....	38
Table 3. 2 Mechanical properties of FRCC.....	41
Table 3. 3 Mixture proportion of concrete used for beam and column .....	41
Table 3. 4 Mechanical properties of concrete.....	41
Table 3. 5 Mechanical properties of rebars .....	42
Table 3. 6 Summary of crack properties at the maximum load.....	50
Table 3. 7 Maximum load and story drift angle at maximum load .....	51
Table 4. 1 Specimens list.....	55
Table 4. 2 Mechanical properties of fiber.....	55
Table 4. 3 Mechanical properties of concrete and PVA FRCC .....	55
Table 5. 1 Parameters for tensile force calculation.....	63
Table 5. 2 Experimental value and calculated value .....	63

## LIST OF FIGURES

Fig. 1. 1 LRV-Precast System.....	9
Fig. 1. 2 Research flow.....	14
Fig. 2. 1 Aramid fiber and PP fiber used in this study.....	19
Fig. 2. 2 Flowability test using funnel.....	20
Fig. 2. 3 Molds for uniaxial tension test specimen.....	20
Fig. 2. 4 Tensile test specimen .....	21
Fig. 2. 5 Notch in the middle of the specimen .....	22
Fig. 2. 6 Cross section of tensile test specimen with notch or without notch.....	22
Fig. 2. 7 Fibers across the crack during loading.....	23
Fig. 2. 8 Tensile stress –axial deformation curve .....	23
Fig. 2. 9 Final condition of cross section of aramid specimens .....	25
Fig. 2. 10 Final condition of cross section of PP specimens .....	25
Fig. 2. 11 Fibers across the crack during loading aramid specimens .....	27
Fig. 2. 12 Fibers across the crack during loading of PP specimens.....	27
Fig. 2. 13 Tensile stress-crack with curve .....	28
Fig. 2. 14 Final condition of cross section of aramid specimens .....	29
Fig. 2. 15 Final condition of cross section of PP specimens .....	30
Fig. 2. 16 Three-point bending test .....	31
Fig. 2. 17 Notched part of three-point bending test.....	31
Fig. 2. 18 Failure patterns of aramid specimens.....	32
Fig. 2. 19 Failure patterns of PP specimens .....	32
Fig. 2. 20 Bending stress – rotation angle curve .....	33
Fig. 2. 21 Four-point bending test .....	33
Fig. 2. 22 Failure patterns of aramid specimens.....	34
Fig. 2. 23 Failure patterns of PP specimens .....	34
Fig. 2. 24 Bending stress – rotation angle curve .....	35
Fig. 3. 1 Casting separately .....	36
Fig. 3. 2 LRV-Precast System.....	37
Fig. 3. 3 Specimen dimensions.....	38
Fig. 3. 4 Foundation platform.....	39
Fig. 3. 5 Mold for panel zone .....	39
Fig. 3. 6 Casting the panel zone .....	39

Fig. 3. 7 Demolding.....	40
Fig. 3. 8 Install lateral reinforcements and the molds .....	40
Fig. 3. 9 Casting beam and column.....	40
Fig. 3. 10 Loading method .....	43
Fig. 3. 11 Measurement of story drift angle .....	43
Fig. 3. 12 Measurement of local deformation .....	44
Fig. 3. 13 Failure patterns.....	45
Fig. 3. 14 Photographing region.....	45
Fig. 3. 15 Details of photographing region .....	46
Fig. 3. 16 Crack patterns of No.25 (PVA).....	46
Fig. 3. 17 Crack patterns of No.30 (aramid) .....	47
Fig. 3. 18 Crack patterns of No.31 (PP) .....	47
Fig. 3. 19 Evaluation of crack properties .....	48
Fig. 3. 20 Crack width.....	48
Fig. 3. 21 Crack opening.....	49
Fig. 3. 22 Crack sliding.....	49
Fig. 3. 23 Principal strain angle and crack angle.....	49
Fig. 3. 24 Summary of crack opening, sliding and width .....	50
Fig. 3. 25 Relationships of load and story drift angle .....	52
Fig. 4. 1 Example of fiber orientation after vibrating.....	53
Fig. 4. 2 Casting directions.....	54
Fig. 4. 3 Example of horizontal casting.....	56
Fig. 4. 4 Example of vertical casting.....	56
Fig. 4. 5 Casting procedures.....	57
Fig. 4. 6 Crack pattern at maximum load.....	58
Fig. 4. 7 Position of main reinforcing bars in column.....	58
Fig. 4. 8 Load-story drift angle curve.....	59
Fig. 4. 9 Comparison of skeleton curves .....	59
Fig. 5. 1 Internal actions into panel zone .....	61
Fig. 5. 2 Calculation of tensile force .....	62
Fig. 5. 3 Calculation of shear force .....	62

## DISSERTATION ABSTRACT

Beam-column joint is the crucial part of a reinforced concrete (RC) frame, which is to ensure the ductility of the whole structure especially when the frame is subjected to huge earthquake. Under seismic response, major damage should be avoided in the beam-column joint. Even the beam and column step into inelastic state, the joint has to remain the ability to transfer actions. The reasons to avoid large damage in beam-column joint under seismic response are to keep transferring capacity of the gravity load in the panel zone, to accomplish large ductility and energy dissipation by other elements such as beam, and difficulty of repair the joint after earthquake.

Shear failure in the panel zone causes a typical brittle damage in beam-column joint, so its shear capacity should be given gratifyingly. Shear capacity of beam-column joint is mainly supplied by the dimensions of the panel zone and concrete strength. An adequate amount of lateral confining reinforcements in the panel zone also provides non-shear failure. In general, however, the dimensions of the panel zone are limited by the dimensions of connecting columns and beams. In addition, increasing confining reinforcements will cause great construction difficulties in reinforcement cage and casting.

Using fiber-reinforced concrete into panel zone of beam-column joint to increase shear capacity is not a new attempt. By the introduction of steel fibers in beam-column joints, steel fiber-reinforced concrete (SFRC) is attractive to inhibit the damage of joint panel and increase maximum load. However, decreased stress caused by steel fiber corrosion is a severe problem that has to be faced. With the development of polymer material, various synthetic fibers have become the best selection to improve concrete capacity and failure resistance without the corrosion of fibers.

A newly cementitious-composite-based material named fiber-reinforced cementitious composite (FRCC) is cement composite with the mixture of short fibers to increase ductility of cement composite. Comparing to the conventional concrete, FRCC has a remarkable deformability especially under tensile and bending load with a large energy absorption capacity due to the fiber bridging effect. After first cracking, fiber can transfer tensile force through crack which strongly affects the tensile performance of FRCC. When fibers tend to orient perpendicularly to crack surface, higher effect of bridging of fibers is observed. When fibers tend

to orient parallel to crack, however, bridging performance of fibers becomes poor.

FRCC consists of a typical self-compacting cementitious matrix with a high viscosity. It has been considered that fresh-state properties, casting method, vibration, flow and framework, etc. have the effect on the orientation of fibers. For tensile characteristics of FRCC, the previous research has already studied the influence of casting direction on the fiber orientation of FRCC through a visualization simulation and higher tensile stress of the second peak was observed in horizontal casting specimens than that of vertical casting specimens.

This remarkable bridging capacity makes FRCC an appropriate choice for application in beam-column joint of RC structures to resist inelastic deformation. Until now, FRCCs can be constituted with a category of fibers, such as carbon, steel and polymer fibers. Whereas, most research in materials field has been focused on FRCC with a high modulus polyethylene (PE) fiber, and has been conducted by bending and tensile test. Structural performance of beam-column joints using polyvinyl alcohol (PVA) and steel fiber in panel zone with a fiber volume fraction of 1% have been confirmed. Fibers can restrain expansion of crack width, increase shear capacity and improve structural performance rather than the specimen without fiber. The previous research has also revealed that PP-ECC (a sort of polypropylene fiber-reinforced cementitious composite) can serve as transverse reinforcements to carry the applied load.

Precast construction method which is widely used in RC buildings especially in high skyscraper in Japan becomes more and more popular by ensuring better quality, simplified install procedure and shorter duration. Until now, a new precast system which casting the joint panel combining with beam and separating column into two parts has been proposed. Even though the FRCC constructability is tough, by adopting this precast method, FRCCs can be used in practical engineering easily. Therefore, it is a smart way of enable FRCC to play a better role in a beam-column joint.

In this study, various polymer fibers have been utilized in the FRCCs beam-column joint to increase shear capacity and reduce the damage of the panel zone. Compared with steel fiber, polymer fibers have a better durability in cement matrix. The loading test of FRCCs beam-column joints with a fiber volume fraction of 1% are conducted to make clear the influence of fiber type on shear capacity of panel zone. The loading test of two PVA FRCC beam-column joints with a fiber volume fraction of 1% are conducted to evaluate the effect of casting direction on structural performance and crack behavior of panel joint by which horizontal casting and vertical casting are applied. Tensile and bending performance of FRCCs characterized from uniaxial tension test

is also discussed. A new calculation method for evaluating shear capacity of FRCCs beam-column joint is proposed based on the standard of Architectural Institute of Japan.

The following is a brief description of the contents of each chapter in the thesis.

#### CHAPTER 1 Introduction

In this chapter, the literature review on the use of FRCC to strength concrete structures and the research background on FRCC beam-column joint are introduced. The research objectives are enumerated, and the research approach is described. Finally, the aims and outline of this doctoral thesis are introduced.

#### CHAPTER 2 Tensile and Bending Behavior of FRCC

FRCCs are a group of cement composites with the mixture of short fibers to increase their ductility and strength by the effect of fiber bridging after first cracking. Though the bending test and uniaxial tension test are usually carried out to characterize their performance, both notched specimens and un-notched specimens have been used for these tests. PVA, aramid and PP fiber are used as 1% volume fraction. The water cement ratio is set to 0.56.

The specimens for uniaxial tension test are divided into two series, i.e., without notch or with notch. The test regions of cross section are 50 mm × 50 mm and 40 mm × 40 mm for the specimens without and with notch, respectively. The total length of the specimen is 510 mm. Pin-fix ends were adopted at the boundaries to minimize possible effects of external moment. Tensile load and deformation in the test region were obtained directly from the experiment. Tensile stress is calculated by considering the different section area of two types of specimens. The tensile behavior after first cracking differs by types of fiber. Except the PP specimen without notch, the tensile stress showed a significant drop after first cracking. Due to the fiber bridging effect, the tensile stress increased until to the second peak and then decreased gradually. For the aramid specimen without notch, multiple cracks were observed after first cracking which leads to the several increase and decrease of tensile stress. In case of the PP specimen without notch, the second peaks could not be measured due to sudden opening over 1 mm crack width. The average tensile stress of aramid specimen with and without notch at second peak is 3.02 MPa and 3.31 MPa, of that for PP specimen is 1.61 MPa and 1.33 MPa, respectively.

The bending test was conducted for same FRCC with uniaxial tension test specimens. Three-point bending test and four-point bending test were carried out separately to obtain the bending

performance of FRCCs. The notched beam specimens (three-point bending test) with 100mm square section specified in JCI-S-002-2003 were used. The notch was cut in the middle of specimen with a depth of 30mm. One LVDT was set to measure the load point deflection. The four-point bending test based on JCI-S-003-2007 was conducted. Three LVDTs were set to measure the load point deflections and the deflection at the center of the specimen. For three-point bending test specimen, the rotation angle is defined as load point deflection divided by half of span (150mm). In case of four-point bending test specimen, the rotation angle is defined as the average of load point deflections divided by shear span (100mm). In order to compare the difference of specimens with or without notch, the bending stress is also defined as bending moment at the load point divided by section modulus. In case of aramid specimens, the load was increased significantly after first cracking to maximum for both types of bending test. For PP specimens, the load dropped after the maximum load and increased gradually again showing second peak load. The average of bending stresses at the maximum load after the sudden drop of the load (second peak) is 4.37 MPa and 5.48 MPa for aramid three-point and four-point specimen. The bending stress of PP specimen at second peak is 2.13 MPa and 2.44 MPa.

The tensile and bending behavior of FRCC has been confirmed from uniaxial tension test and bending test directly by specimens with or without notch. The maximum tensile stresses for PVA, aramid and PP specimens are  $1.80 \text{ N/mm}^2$ ,  $3.02 \text{ N/mm}^2$  and  $1.61 \text{ N/mm}^2$  which could be used to evaluate the structural performance of FRCC.

### CHAPTER 3 Influence of Fiber Types on Structural Performance of FRCC Beam-Column Joints

With the development of polymer material, various synthetic polymer fibers have become the best selection to improve concrete capacity and failure resistance without corrosion of fibers. The influence of fiber types on tensile and bending performance of FRCC has been confirmed in Chapter 2. In this Chapter, aramid and PP fibers were used as 1% volume fraction in panel zone to seek the influence of fiber types on structural performance of FRCC beam-column joint. The results of beam-column joint without fiber and beam-column joint using PVA FRCC are also included to compare with aramid and PP FRCC beam-column joints.

Two specimens (aramid and PP) were designed to fail by shear in panel zone before flexural yielding to evaluate the shear performance of joint panel. The reversed cyclic loading is applied to the beams controlling story drift angles from  $R = \pm 1/400$  to  $\pm 1/20$  rad. The results of similar specimens using PVA fiber tested in previous study are also discussed together. Comparing with specimen without fiber, the damage of specimens with fibers is inhibited due to the effect of fiber

bridging. The maximum loads of beam-column joints increase by adding fiber. Specimen No.30 has the highest maximum load which is 544kN. It is recognized that the bridging effect is different by types of fiber.

#### CHAPTER 4 Influence of Casting Method on Structural Performance of FRCC Beam-Column Joints

To clarify the influence of fiber orientation on structural performance of PVA FRCC beam-column joint by using two types of casting method, horizontal and vertical casting beam-column joint specimens are tested by reversed cyclic load simulating earthquake force. A vibrator rod is also applied during the casting.

PVA fiber is used for all specimens with a fiber volume fraction of 1%. Two types of casting method, which is horizontal casting and vertical casting were used. During the casting, a vibrator rod was being inserted into the matrix along with the direction of casting to arrange the fiber orientation of panel zone. The testing parameter is the casting direction along the horizontal and vertical directions. The dimensions of specimens and loading method are as same as mentioned in Chapter 3.

The maximum load of horizontal casting specimen was observed at the cycle of 1/50 rad and that of vertical casting specimen was at 1/67 rad. After the maximum load, although the crack width increased with the increase of story drift angle, damage of joint panel was inhibited by the fiber bridging effect comparing to specimen without fiber. From the comparison between horizontal specimen and vertical specimen, of which maximum load is 461kN and 468kN respectively. This indicates that casting direction of panel zone do not affect shear capacity of PVA FRCC beam-column joint significantly. Specimens of horizontal casting and vertical casting show almost the same shear capacities.

#### CHAPTER 5 Evaluation of Shear Capacity of FRCC Beam-Column Joints

By assuming that the shear stress in the panel zone is also carried by fiber bridging effect, shear capacity of beam-column joint is evaluated through the tensile characteristics of FRCC.

It is considered that the strut mechanism in FRCC beam-column joint keeps until to story drift angle of  $R=1/50$ rad due to the bridging effect of fibers which are across the diagonal crack on the surface of panel zone. After that, diagonal cracks start to move to shear sliding direction which leads to the maximum load. At the maximum load, by assuming failure of strut mechanism and disappear of fiber bridging effect are occurred simultaneously, calculation method for shear capacity of FRCC beam-column joint can be proposed as the summation of the value given by

*Design Guidelines for Earthquake Resistant Reinforced Concrete Buildings Based on Inelastic Displacement Concept* and shear force carried by FRCC. The second peak load in uniaxial tension test are adopted for maximum tensile stress in each type of fibers.

Experimental and calculated values of shear capacity are converted to the shear force which is applied to beam. The difference of below 7% between calculated value and experimental value demonstrates that the calculation method is feasible. By adopting this method, shear capacity of FRCC beam-column joint can be calculated from uniaxial tension test.

#### CHAPTER 6 Conclusions

The retrospective view of this research objectives and the conclusions drawn from this work have been summarized. Recommendations for future research are also highlighted in this chapter.

## CHAPTER 1 Introduction

### 1.1 Research Background

It is generally known that concrete is a brittle material due to the quite lower tensile strength than the compressive strength. In reinforced concrete (RC) structures, it is expected that the compressive force is carried by concrete and the tensile force is carried by reinforced rebars. Brittle failure in RC members is mainly due to tensile fracture of concrete. For example, bond splitting failure in which the integrity of concrete and reinforcing bar impaired is also due to the low tensile performance of concrete. In order to improve the tensile performance, attempts have been made to ensure the toughness of mortar and concrete by incorporating short fibers with a length of several to several tens of millimeters during the past few decades [1.1]. Such these materials have named as fiber-reinforced cementitious composites (FRCCs). The fibers used in FRCC are mainly divided into three categories: natural fibers, inorganic fibers and polymer fibers.

Natural fibers are consisted of animal-based, mineral-derived and plant-based fibers. These fibers are renewable sources which have been renewed by nature and human ingenuity for thousands of years [1.2]. Natural fibers are environment friendly, completely renewable, low density, non-abrasive, bio-degradable, low cost and local availability [1.3-1.5]. However, scattering performance of natural fibers caused by un-controlled manufacturing process which limited the use of natural fibers [1.6].

Steel fiber is a typical type of inorganic fibers, which has a higher strength compared to natural fibers. Steel fiber-reinforced concrete (SFRC) is gradually being used for auxiliary reinforcement for temporary conditions and partial replacement of conventional reinforcement [1.7-1.9]. Under certain circumstances, the use of steel fibers to replace partial or total conventional reinforcing bars has become a good choice for the construction of precast section lining of bored tunnel [1.10,1.11]. However, the long-term durability of SFRC under chloride and carbonation is a severe problem that has to be faced [1.12-1.14]. The damage of fiber bridging at fiber-matrix interface of steel fiber-reinforced cementitious composite (SFRCC) exposed to corrosive environment conditions has been confirmed by many researchers [1.15].

With the development of polymer material, various synthetic polymer fibers have become the best selection to improve concrete capacity and failure resistance without corrosion of fibers [1.16]. Polymer fibers, such as polyethylene (PE), polyvinyl alcohol (PVA), polypropylene (PP) and aramid fiber, can be used for reinforcement and to offer mechanical support to concrete. A tensile strength exceeding 5.5 MPa and tensile strain capacity of 6% of engineered cementitious composite (ECC) with 1.5% by volume fraction has been confirmed. The strain-hardening

behavior after first cracking results in an improvement in toughness and ductility [1-17,1-18]. PVA fiber is also widely used due to the feature of high interfacial chemical bond behavior between fiber and matrix. High friction stress is observed in case of PVA fiber which ensures the slip-hardening ability in cementitious matrix. PVA-ECC with a fiber volume fraction of 2% achieved tensile strength of 4.5 MPa and ultimate strain of 4% [1.19]. Aramid fibers having an extraordinary tensile strength of over 2000 MPa have been used in aircraft, military vehicles, bullet proof vests and many other. The low cost of PP fibers makes it to be used for FRCC. Such these polymer fibers are expected to be used to improve the capacity of the key parts of in real RC structures.

Beam-column joint is the crucial part of a RC frame, which is to ensure the ductility of the whole structure especially when the frame is subjected to huge earthquake. Under seismic response, major damage should be avoided in the beam-column joint. Even the beam and column step into inelastic state, the joint has to remain the ability to transfer actions. The reasons to avoid large damage in beam-column joint under seismic response are to keep transferring capacity of the gravity load in the panel zone, to accomplish large ductility and energy dissipation by other elements such as beam, and difficulty of repair the joint after earthquake [1.20].

Shear failure in the panel zone causes a typical brittle damage in beam-column joint, so its shear capacity should be given gratifyingly. Shear capacity of beam-column joint is mainly supplied by the dimensions of the panel zone and concrete strength. An adequate amount of lateral confining reinforcements in the panel zone also provides non-shear failure. In general, however, the dimensions of the panel zone are limited by the dimensions of connecting columns and beams. In addition, increasing confining reinforcements will cause great construction difficulties in reinforcement cage and casting.

Comparing to the conventional concrete, FRCC has a remarkable deformability especially under tensile and bending loading with large energy absorption capacity due to the effect of fiber bridging is expected to be used in the crucial part of a RC frame to improve the structural performance. However, according to the flowability of cementitious composites during casting, fiber clustering is an avoidable problem for the application of FRCC. Since the FRCC is very expensive, it could be only used in the panel zone of beam-column joint. Separated casting of panel zone from beam and column is required for making of FRCC beam-column joint. Such difficulties limit the utilization of FRCC into a real RC frame.

Precast construction method which is widely used in RC buildings especially in high skyscraper

in Japan becomes more and more popular by ensuring better quality, simplified install procedure and shorter duration. Until now, a new precast system which casting the joint panel combining with beam and separating column into two parts has been proposed [1.21]. Even though the FRCC constructability is tough, by adopting this precast method, FRCCs can be used in practical engineering easily. Therefore, it is a smart way of enable FRCC to play a better role in a beam-column joint.

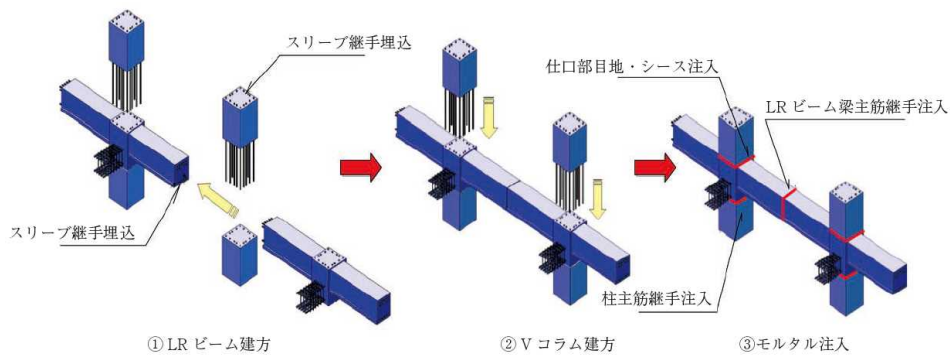


**Fig. 1. 1 LRV-Precast System [1.21]**

In this research, various polymer fibers have been utilized in the FRCCs beam-column joint to increase shear capacity and reduce the damage of the panel zone. Compared with steel fiber, polymer fibers have a better durability in cement matrix. The loading test of FRCCs beam-column joints with a fiber volume fraction of 1% are conducted to make clear the influence of fiber type on shear capacity of panel zone. Tensile performance of FRCCs characterized from uniaxial tension test is also discussed. A new calculation method for evaluating shear capacity of FRCCs beam-column joint is proposed based on the standard of Architectural Institute of Japan.

## 1.2 Literature Review

Using fiber-reinforced concrete (FRC) into panel zone of beam-column joint to increase shear capacity is not a new attempt. This section introduces the literature review related to this research conducted to date.

Henager, C. H., designed and tested two seismic-resistant joints to confirm the possibility of minimizing steel congestion in joint. Experimental comparison was performed on two full-scale beam-column joints. One was with conventional reinforcing hoops and the other was a modified joint using steel fiber in joint area to replace the use of hoops. The two joints were subjected under loading of two major typical earthquakes. The SFRC beam-column joint had a higher ultimate

moment capacity and high stiffness compared to the conventional joint. Better damage tolerance and crack resistance of SFRC beam-column joint were observed. The reduced steel congestion makes the manufacture of the joint simpler. It is considered that using FRCC into joint can save US\$ 100 per joint [1.22].

Halvorsen, G. T., *et al* reported that cracking of the matrix caused by pullout of the fibers would result in the failure of SFRC beams. Ordinary steel fiber and deformed steel fiber were adopted to compare the performance of 100 mm x 150 mm x 1625 mm SFRC beams. The specimens using deformed fibers showed higher flexural strength which indicated that fibers must be ductile and have a better pullout resistance [1.23].

Craig, R. *et al* conducted ten beam-column joints of which half of these joints using steel hooked end fibers of volume fraction of 1.5% to study the failure conditions. Through the analyzing the test results, it can be confirmed that the steel fibers with hook-shaped ends in the joint panel has: 1) better interfacial bond; 2) better confinement compared with hoops; 3) more stiffer structures 4) higher moment capacity; 5) higher shear strength; 6) more ductile; 7) compared with ordinary concrete joints, the energy dissipation capacity has been significantly improved [1.24].

Naaman, A. E., *et al* introduced a framing system with high fiber content reinforced concrete as the primary matrix in the case-in-place joint which is to ensure higher ductility, increase the energy absorption reduce spalling, and improve shear capacity resisted reversed cyclic loading [1.25].

Gefken, P. R. *et al* tested ten beam-column joints to study whether using SFRC could replace ordinary concrete in the joint panel. The results indicated that the joint hoop spacing could be increased by using fiber in joint area. The specimens with fibers showed very little or no spalling of concrete, however, extensive spalling of concrete was observed in case of specimens using normal concrete [1.26].

Jiuru, T., *et al* made clear that SFRC increases the shear strength of joint, energy dissipation capacity and ductility through 12 beam-column joints test. The influence of reinforcement ratio, the volume ratio of the stirrups and the beam bar length was also discussed. Experimental results revealed that using SFRC in panel zone could minimize the influence of congestion of steel reinforcement in a beam-column joint. A better bond performance and the improvement of anchorage behavior were confirmed by using FRCC in the beam-column joint. A formula to

describe the shear strength of SFRC beam-column joint has been proposed [1.27].

Durrani, A. J., *et al* discussed the effect of fiber-reinforcement on the seismic behavior of three half-scale interior and exterior connections. Ductile low carbon steel was used. The energy dissipation capacity and ductility were increased significantly due to the addition of fiber reinforcement. The seismic response was improved by adding fiber to slab-column connections [1.28].

Filiatrault, A. *et al* represented three full-scale interior beam-column joints which is normal concrete specimen, specimen equipped with full seismic details, and normal concrete specimen included hook-end steel fibers in the joint corn area. The test results revealed that the shear strength of joint was increased by fibers bridging across the crack meanwhile closely spaced ties could be achieved [1.29].

By the introduction of steel fibers in beam-column joints, SFRC is an attractive choice to inhibit the damage of joint panel and increase maximum load. However, decreased stress caused by steel fiber corrosion [1.30,1.31] is a severe problem that has to be faced. The effect of corrosion was studied by measurement of fiber corroded surface, evaluation of minimum fiber diameter after exposure, and toughness. The experimental results showed that the strength and toughness decreased after a part of corrosion was occurred which led to the degradation of total mechanical properties. Furthermore, a much more dramatic decrease in toughness and strength happened in the case of a certain level of exposure. According to the above researches, although SFRC could be used in beam-column joint or other crucial parts of RC structures, the corrosion of steel fiber limits the use of SFRC.

With the development of polymer material, various synthetic polymer fibers have become the best selection to improve concrete capacity and failure resistance without corrosion of fibers [1.32]. Polymer fibers, such as PE, PVA, PP and aramid fiber, can be used for reinforcement and to offer mechanical support to concrete.

Comparing to the conventional concrete, FRCC has a remarkable deformability especially under tensile and bending load with a large energy absorption capacity due to the fiber bridging effect. After first cracking, fiber can transfer tensile force through crack which strongly affects the tensile performance of FRCC. Kanakubo, T., *et al* pointed out that fiber orientation strongly affects the tensile performance of FRCC after cracking. The visualization simulation using water glass solution and uniaxial tension test of two types of specimens were conducted. Horizontal

casting specimens had an average tensile stress of 3.51 MPa which is more than 2 times of the corresponding value of the vertical casting specimens. A bridging law which is to describe the fiber crack bridging behavior was also proposed [1.33].

Sano, N., has reported that the damage of beam-column joint was inhibited and the shear capacity was increase by the fiber bridging effect though a loading test of two beam-column joint specimens. The crack width was measured by taking photos of the surface of beam-column joint every 10 seconds. Due to the shear force is determined by crack width and principal strain angle, the shear capacity was evaluated by tensile stress calculated from bridging law. The calculated value showed a similar tendency with the shear force increment obtained from experiment [1.34].

Yamada, H., compared six beam-column joints containing the specimens without fiber, specimens with PVA fibers, and specimens with steel fibers. The shear capacity of steel fiber reinforced beam-column joint was higher than that of the specimen with PVA fiber. And also, the photos of the surface of beam-column joint were taken every 10 seconds to measure the crack width and principal strain angle. According to the calculation, in the case of PVA specimens, the calculated shear force agreed with the experimental results. However, the calculated shear force of specimens with steel fiber disagreed with the test results [1.35].

Zhang, R., applied PP-ECC in beam-column joint connections of rigid-framed railway bridge to reduce stirrups and hoops. The reverse cyclic loading test of beam-column joints and four-point bending test were conducted to study the effects of PP fibers on shear capacities of PP-ECC applications. The results indicated that PP-ECC could take place of the transverse reinforcements in beam-column joint to carry the applied load [1.36].

This remarkable bridging capacity makes it an appropriate choice for application in beam-column joint of RC structures to resist inelastic deformation. Fibers can restrain expansion of crack width, increase shear capacity and improve structural performance rather than the specimen without fiber. However, most researches have been conducted on structural performance of SFRC members and material test of FRCC using polymer fibers. More studies should be carried out to investigate the influence of polymer fibers on structural performance of FRCC members. Therefore, it is important to conduct more material tests and beam-column joint tests of FRCC specimens using polymer fibers.

### 1.3 Objective and Scope

Although researches on FRCC beam-column joint have been extensively conducted, as

mentioned before, the substantial existing researches mostly focus on FRCC using steel fibers. The experimental study of FRCC beam-column joint using polymer fibers deserved more attention. Therefore, the principal objective and scope of this thesis research are as follow:

First, the tensile and flexural characteristics of FRCC using various polymer fibers were investigated. The maximum tensile stress of FRCC was obtained directly from the uniaxial tension test which could be used to predict the shear capacity of FRCC beam-column joint.

Second, beam-column joint test under reversed cyclic loading was carried out to examine the shear performance of FRCC beam-column joints. The different failure patterns of beam-column joints with each type of fibers were observed. The relationship of load and story drift angle of each specimen was obtained directly from the experiments. The influence of fiber types on shear behavior of FRCC beam-column joints was discussed.

Next, the influence of casting directions on shear performance of FRCC beam-column joints was examined. Two types of casting directions which are horizontal casting and vertical casting were adopted for the fabrication of specimens. The influence of casting directions on shear capacity of FRCC beam-column joints was studied.

Finally, a new calculation method for evaluating shear capacity of FRCCs beam-column joint was proposed based on the standard of Architectural Institute of Japan [1.37].

## 1.4 Outline of the Thesis

The flow of this research is shown Fig. 1.2.

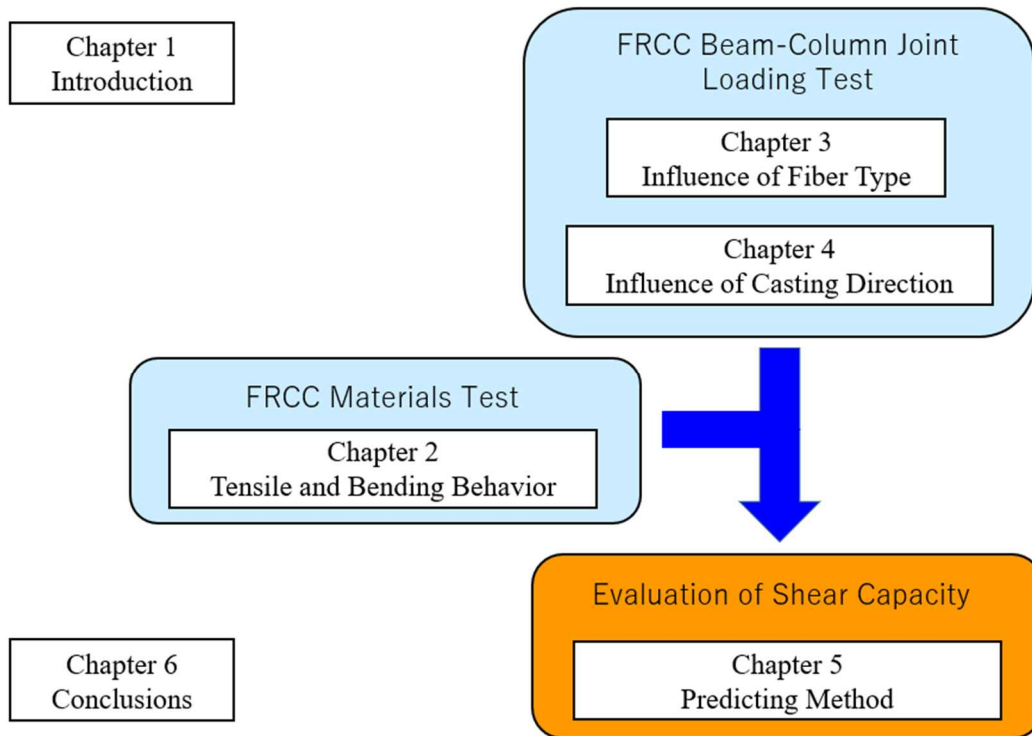


**Fig. 1. 2 Research flow**

The following is a brief description of the contents of each chapter in the thesis.

### CHAPTER 1 Introduction

In this chapter, the literature review on the use of FRCC to strength concrete structures and the research background on FRCC beam-column joint are introduced. The research objectives are enumerated, and the research approach is described. Finally, the aims and outline of this doctoral thesis are introduced.

### CHAPTER 2 Tensile and Bending Behavior of FRCC

The bending test and uniaxial tension test are carried out to characterize FRCCs' performance, both notched specimens and un-notched specimens have been used for these tests. PVA, aramid and PP fiber are used as 1% volume fraction. The water cement ratio is set to 0.56.

The specimens for uniaxial tension test are divided into two series, i.e., without notch or with

notch. The test region of cross section is 50 mm × 50 mm and 40 mm × 40 mm for the specimens without and with notch, respectively. The total length of the specimen is 510mm. Pin-fix ends were adopted at the boundaries to minimize possible effects of external moment. Tensile load and deformation in the test region were obtained directly from the experiment. Tensile stress is calculated by considering the different section area of two types of specimens. The tensile behavior after first cracking differs by types of fiber. Except the PP specimen without notch, after a significant drop of tensile stress at first cracking, the tensile stress increased until to the second peak and then decreased gradually. For the aramid specimen without notch, multiple cracks were observed after first cracking which leads to the several increase and decrease of tensile stress. In case of the PP specimen without notch, the second peaks could not be measured due to sudden opening over 1mm crack width. The average tensile stress of aramid specimen with and without notch at second peak is 3.02 MPa and 3.31 MPa, respectively. While the average tensile stress of PP specimen with notch at second peak is 1.61 MPa, the average stress after sudden crack opening in PP specimen without notch is 1.33 MPa.

The bending test was conducted for same FRCC with uniaxial tension test specimens. Three-point bending test and four-point bending test were carried out separately to obtain the bending performance of FRCCs. The notched beam specimens (three-point bending test) with 100mm square section specified in JCI-S-002-2003 were used. The notch was cut in the middle of specimen with a depth of 30mm. One LVDT was set to measure the load point deflection. The four-point bending test based on JCI-S-003-2007 was conducted. Three LVDTs were set to measure the load point deflections and the deflection at the center of the specimen. For three-point bending test specimen, the rotation angle is defined as load point deflection divided by half of span (150mm). In case of four-point bending test specimen, the rotation angle is defined as the average of load point deflections divided by shear span (100mm). In order to compare the difference of specimens with or without notch, the bending stress is also defined as bending moment at the load point divided by section modulus. In case of aramid specimens, the load was increased significantly after first cracking to maximum for both types of bending test. For PP specimens, the load dropped after the maximum load and increased gradually again showing second peak load. The average of bending stresses at the maximum load after the sudden drop of the load (second peak) is 4.37 MPa and 5.48 MPa for aramid three-point and four-point specimen. The bending stress of PP specimen at second peak is 2.13 MPa and 2.44 MPa.

The tensile and bending behavior of FRCC has been confirmed from uniaxial tension test and bending test directly by specimens with or without notch. The maximum tensile stresses for PVA, aramid and PP specimens obtained from uniaxial tension test specimens with notch are 1.80 MPa,

3.02 MPa and 1.61 MPa which could be used to evaluate the structural performance of FRCC.

#### CHAPTER 3 Influence of Fiber Types on Structural Performance of FRCC Beam-Column Joints

The influence of fiber types on tensile and bending performance of FRCC has been confirmed in Chapter 2. In this Chapter, aramid and PP fibers were used as 1% volume fraction in panel zone to seek the influence of fiber types on structural performance of FRCC beam-column joint. The results of beam-column joint without fiber and beam-column joint using PVA FRCC are also included to compare with aramid and PP FRCC beam-column joints.

Two specimens (aramid and PP) were designed to fail by shear in panel zone before flexural yielding to evaluate the shear performance of joint panel. The reversed cyclic loading is applied to the beams controlling story drift angles from  $R = \pm 1/400$  to  $\pm 1/20$  rad. The results of similar specimens using PVA fiber tested in previous study are also discussed together. Comparing with specimen without fiber, the damage of specimens with fibers is inhibited due to the effect of fiber bridging. The maximum loads of beam-column joints increase by adding fiber. Specimen with aramid fiber (No. 30) has the highest maximum load which is 544 kN. It is recognized that the bridging effect is different by types of fiber.

#### CHAPTER 4 Influence of Casting Method on Structural Performance of FRCC Beam-Column Joints

To clarify the influence of fiber orientation on structural performance of PVA FRCC beam-column joint by using two types of casting method, horizontal and vertical casting beam-column joint specimens are tested by reversed cyclic load. A vibrator rod is also applied during the casting.

PVA fiber is used for all specimens with a fiber volume fraction of 1%. Two types of casting method, which is horizontal casting and vertical casting were used. During the casting, a vibrator rod was being inserted into the matrix along with the direction of casting to arrange the fiber orientation of panel zone. The testing parameter is the casting direction along the horizontal and vertical directions. The dimensions of specimens and loading method are as same as mentioned in Chapter 3.

The maximum load of horizontal casting specimen was observed at the cycle of  $1/50$  rad. and that of vertical casting specimen was at  $1/67$  rad. After the maximum load, although the crack width increased with the increase of story drift angle, damage of joint panel was inhibited by the fiber bridging effect comparing to specimen without fiber. From the comparison between

horizontal specimen and vertical specimen, maximum load is 461 kN and 468 kN respectively. This indicates that casting direction of panel zone do not affect shear capacity of PVA FRCC beam-column joint significantly. Specimens of horizontal casting and vertical casting show almost the same shear capacities.

#### CHAPTER 5 Evaluation of Shear Capacity of FRCC Beam-Column Joints

By assuming that the shear stress in the panel zone is also carried by fiber bridging effect, shear capacity of beam-column joint is evaluated through the tensile characteristics of FRCC.

It is considered that the strut mechanism in FRCC beam-column joint keeps until to story drift angle of  $R = 1/50$ rad. due to the bridging effect of fibers which are across the diagonal crack on the surface of panel zone. After that, diagonal cracks start to move to shear sliding direction which leads to the maximum load. At the maximum load, by assuming failure of strut mechanism and disappear of fiber bridging effect are occurred simultaneously, calculation method for shear capacity of FRCC beam-column joint can be proposed as the summation of the value given by Design Guidelines for Earthquake Resistant Reinforced Concrete Buildings Based on Inelastic Displacement Concept and shear force carried by FRCC. The second peak loads in uniaxial tension test by notched specimens are adopted for maximum tensile stress in each type of fibers.

Experimental and calculated values of shear capacity are converted to the shear force which is applied to beam. The difference of below 7% between calculated value and experimental value demonstrates that the calculation method is feasible. By adopting this method, shear capacity of FRCC beam-column joint can be calculated from uniaxial tension test.

#### CHAPTER 6 Conclusions

The retrospective view of this research objectives and the conclusions drawn from this work have been summarized. Recommendations for future research are also highlighted in this chapter.

## **CHAPTER 2 Tensile and Bending Behavior of FRCC**

### **2.1 Introduction**

FRCC is cementitious composite with the mixture of short fibers to increase ductility. Comparing to the conventional concrete, FRCC has a remarkable deformability especially under tensile and bending load with a large energy absorption capacity due to the fiber bridging effect. After first cracking, fiber can transfer tensile force through crack which strongly affects the tensile and bending performance of FRCC. However, more researches are necessary to study this fiber contribution of fiber bridging effect to cementitious composite to make clear the influence of fiber types on tensile and bending behavior of FRCC.

In case of ordinary concrete, tensile characteristics are unimportant in the design procedure, which resulted that the standardization of tensile test and evaluation method has been ignored. Due to the difficulties of precise molds and special loading jigs, the uniaxial tension test is hard to conduct to obtain the tensile behavior directly. Generally, the splitting test and three-point bending test are options taking a place of uniaxial tension test. The uniaxial tension test requires special loading devices [2.1]. And also the load transmitting mechanism and boundary condition are considered as factors on the success of uniaxial tension tests [2.2]. Failure at the ends of a specimen should be avoided during loading. The bending moment occurs in case of the precision of specimen shapes, non-uniformity of material itself, setup condition of specimens and stiffness of loading machine [2.3]. The pin-fix boundary condition could minimize the effect external bending moment and the occurring cracks from one side of specimen shall be avoided. Furthermore, smaller specimens have tendency of showing higher strength both in case of cementitious composite materials and conventional concrete materials.

In this chapter, the bending test and uniaxial tension test are carried out to characterize their performance, both notched specimens and un-notched specimens have been used for these tests. PVA, aramid and PP fiber are used as 1% volume fraction. The maximum tensile stresses for PVA, aramid and PP specimens obtained from the uniaxial tension test by notched specimens could be used to evaluate the structural performance of FRCC.

## 2.2 Uniaxial Tension Test

### 2.2.1 Outline of experiment

#### 2.2.1.1 Material properties

Aramid fiber and PP fiber were used to test the tensile property of FRCC. Fiber volume fraction for each specimen was 1%. The photos and mechanical properties of each polymer fibers are shown in Fig. 2.1 and Table 2.1. Aramid fiber and PP fiber are cut with a same length of 30 mm, while 12 mm for PVA fiber. Diameter for Aramid and PP is 0.5 mm and 0.7 mm independently. Aramid fiber has an extraordinary tensile strength of 3432 N/mm<sup>2</sup>. The used aramid fiber was stranded from single fibers. Surface roughness embossing has been made on the PP fiber to improve the bond property.

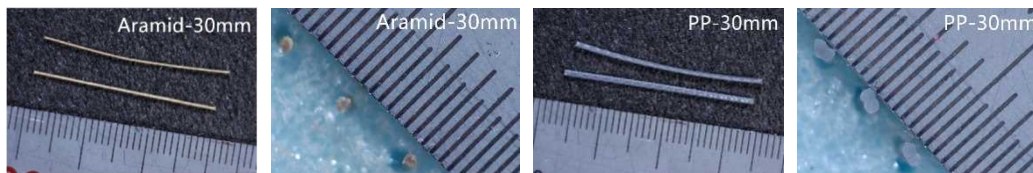


**Fig. 2. 1 Aramid fiber and PP fiber used in this study**

**Table 2. 1 Mechanical properties of fiber**

ID	Fiber	Length (mm)	Diameter (mm)	Tensile strength (MPa)	Elastic modulus (GPa)
No.30	Aramid	30	0.5	3432	73
No.31	PP	30	0.7	580	4.6

The mixture proportion of mortar matrix is listed in Table 2.2. In order to get a better mixture of cementitious composites, higher water-cement ratio of 0.56 was adopted which is based on the previous study [2.4]. High-early-strength Portland cement was used. The rheology of mortar matrix before mixing the fiber is inspected by the flow time [2.5]. As shown in Fig. 2.2, the flow time is measured using a funnel based on “Test method for flowability of grout for prestressing tendons (JSCE-F531-2013)” [2.6]. The time of pouring cementitious matrix was controlled to be a constant to ensure good distribution of fibers. As listed in Table 2.3, compressive strength of aramid and PP specimens was 51.3 MPa and 51.5 MPa by testing of 100 × 200 mm cylinder test specimens (ID corresponds to the beam-column joint specimen in Chapter 3).

**Table 2. 2 Mixture proportion of FRCC**

Fiber volume fraction (%)	Water-binder ratio	Sand-binder ratio	Unit weight (kg/m <sup>3</sup> )			
			Water	Cement	Fly ash	Sand
1.0	0.39	0.50	380	678	291	484

Notes: Cement is high-early-strength Portland cement; fly ash is Type II of Japanese Industrial Standard (JIS A 6202); sand is size under 0.2mm; high-range water-reducing admixture is binder × 0.6%.



**Fig. 2. 2 Flowability test using funnel**

**Table 2. 3 Mechanical properties of concrete**

ID	Fiber	Compressive strength (MPa)	Elastic modulus (GPa)
No. 30	Aramid	51.3	17.7
No. 31	PP	51.5	17.2

As shown in Fig. 2.3, the molds were slanted with 1/33 slope in order to obtain a uniform fiber orientation, the cementitious matrix was pouring into the mold from upper side.



**Fig. 2. 3 Molds for uniaxial tension test specimen**

### 2.2.1.2 Test specimens and loading measurement

The details of the specimen and the loading method are shown in Fig. 2.4. The total length of the specimen is 510 mm with carbon fiber sheets attached at both ends to avoid peel-off of the steel plate. Since the increasing external moment caused by setup irregularity and local fracture caused by secondary moment will be an inevitable factor to the experiment, pin-fix ends were applied at the boundaries to minimize possible effects to the results. Types of specimens were designed to verify the tensile performance of FRCC: specimen with notch and without notch. As shown in Fig. 2.5, a notch was being made in the middle of the specimen after removing the mold. The depth of notch is 5mm. The cross section of the test area is 50 mm × 50 mm for specimen without notch. The sectional area at ligament is 40 mm × 40 mm in case of specimen with notch. Fig. 2.6 shows the cross section of tensile test specimen with notch or without notch.

The test parameters are types of fiber and specimen with or without notch. A 2000 kN universal loading machine was used. Tensile load and axial deformation in the test region were obtained directly from the experiment. The crack width is assumed to be the average value of two pi-type LVDTs in case of notched specimen.

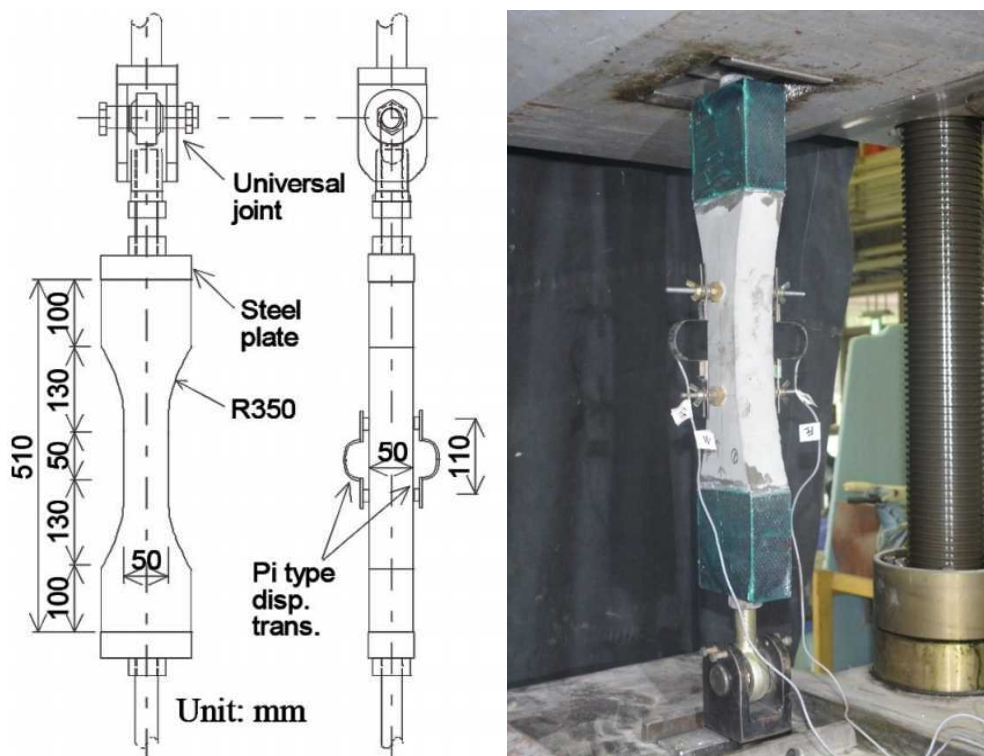
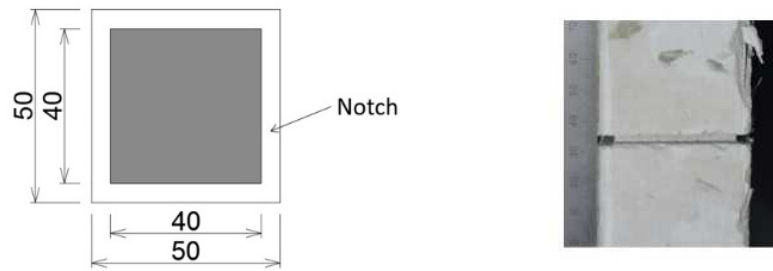
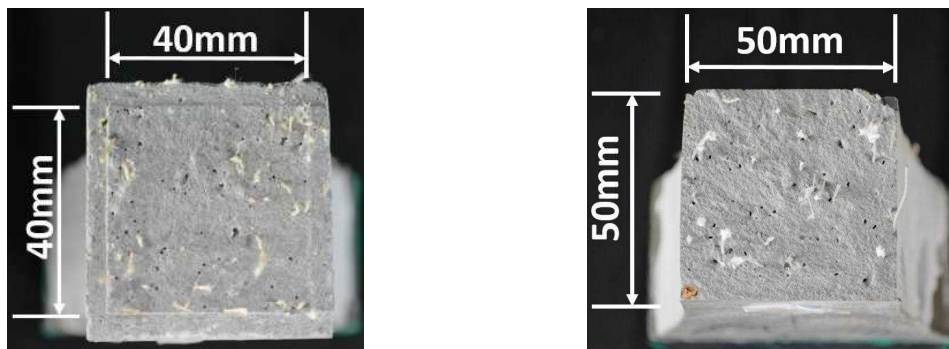


Fig. 2. 4 Tensile test specimen



**Fig. 2. 5 Notch in the middle of the specimen**



**Fig. 2. 6 Cross section of tensile test specimen with notch or without notch**

## 2.2.2 Experimental results and discussion

### 2.2.2.1 Test results for specimen without notch

The example photographs of the fibers across the crack during loading are shown in the Fig. 2.7. Several cracks were observed in case of aramid specimens without notch. For PP specimens without notch, only one crack was observed during loading. The tensile stress is calculated by tensile load divided by cross sectional area. The relationships of tensile stress versus axial deformation are shown in Fig. 2.8. The test results are summarized in Table 2.4.

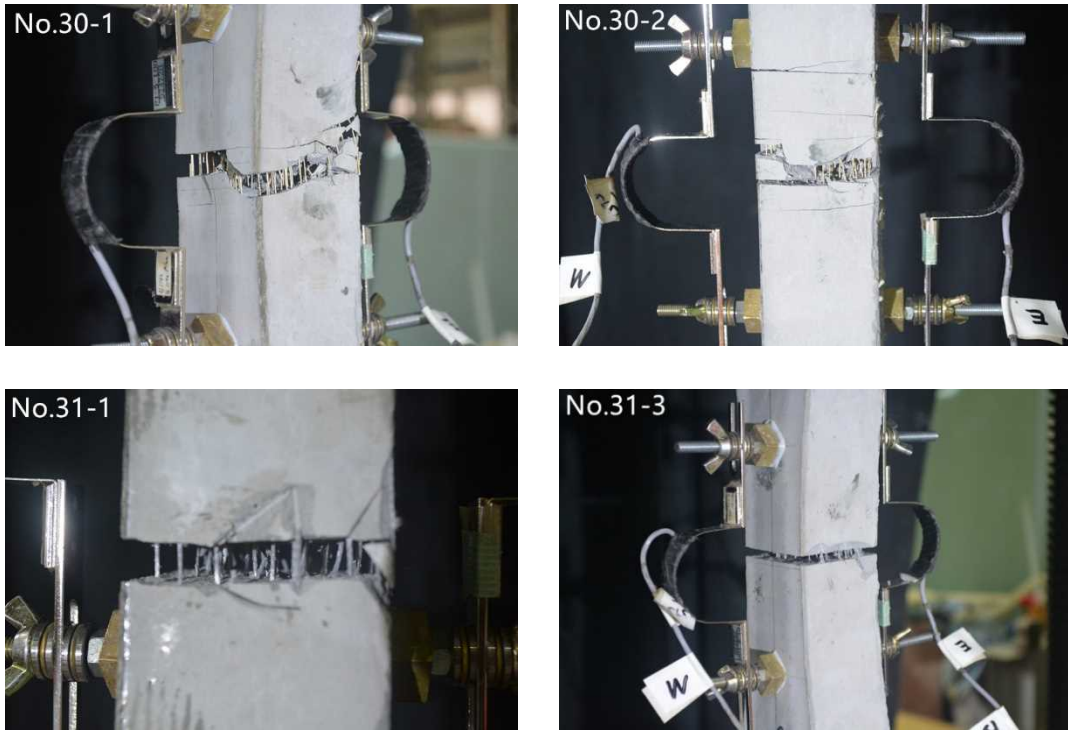


**Fig. 2. 7 Fibers across the crack during loading**

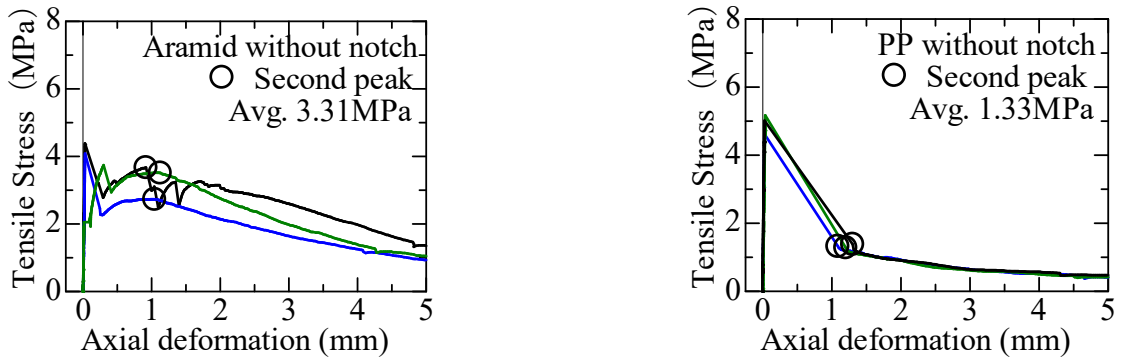


**Fig. 2. 8 Tensile stress –axial deformation curve**

The tensile behavior after first cracking differs by types of fiber. For the aramid specimen without notch, multiple cracks were observed after first cracking which leads to the several increase and decrease of tensile stress. In case of the PP specimen without notch, the second peaks could not be measured due to sudden opening over 1mm crack width. The second peak for PP specimens is defined as the maximum load after cracking which the turning point as shown in Fig. 2.8.

**Table 2. 4 Tensile test results of specimens without notch**

ID		At first cracking (first peak)		Maximum after cracking (second peak)	
		Tensile stress (MPa)	Axial deformation (mm)	Tensile stress (MPa)	Axial deformation (mm)
Aramid	No.30-1	3.74	0.300	3.51	1.126
	No.30-2	4.39	0.029	3.67	0.918
	No.30-4	4.08	0.031	2.73	1.044
	Average	4.07	0.120	3.31	1.029
PP	No.31-1	5.01	0.025	1.38	1.301
	No.31-3	4.62	0.026	1.32	1.087
	No.31-4	5.17	0.035	1.28	1.201
	Average	4.93	0.029	1.33	1.196

The formula expressing the total number of fibers across section in the case of ideal condition can be given by Eq. (2.1). The calculated total number of fibers for aramid specimen and PP specimen is 127.4 and 65.0. The final condition of cross section are shown in the Fig. 2.9 and Fig. 2.10. The bridging fibers across the section were counted after loading. The total numbers of fiber from up side and bottom side are listed in Table. 2.5.

$$N_f = V_f \cdot A_m / A_f \quad (2.1)$$

where  $N_f$  is the calculated total number of fibers,  $V_f$  is fiber volume fraction,  $A_m$  is cross section area of specimen,  $A_f$  is the section area of fiber.

The total number of fibers for specimen No.30-1, No.30-2 and No.30-4 are 158, 183 and 132 which leads to No.30-2 has the highest tensile strength and No. 4 has the lowest tensile strength among the aramid specimens. In the case of PP specimens, the number of fibers is basically the same in three specimens. The total counted number of fibers of aramid specimens is more than the calculated value.



**Fig. 2. 9 Final condition of cross section of aramid specimens**

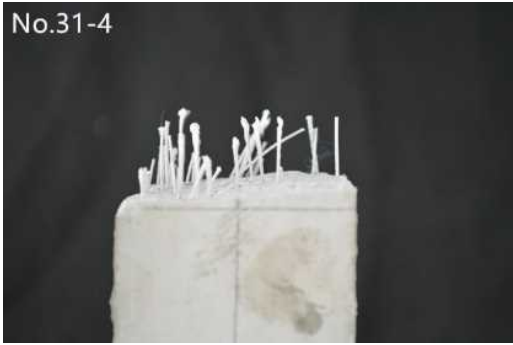


**Fig. 2. 10 Final condition of cross section of PP specimens**

**Table 2. 5 Counted total number of fiber across section of specimens without notch**

ID		Numbers of fiber across section					
		Up side		Bottom side		Total (Up+Bottom)	
		Of each	Average	Of each	Average	Of each	Average
Aramid	No.30-1	75	76.3	83	81.3	158	157.7
	No.30-2	87		96		183	
	No.30-4	67		65		132	
PP	No.31-1	28	29.0	28	29.3	56	58.3
	No.31-3	23		23		46	
	No.31-4	36		37		73	

#### 2.2.2.2 Test results for specimen with notch

In order to compare the structural performance of FRCC members using other polymer fiber, PVA fiber with a tensile strength of 1200 MPa which is the same as previous research [2.7] was also used in the case of specimens with notch. The length of PVA fiber is 12mm and the diameter is 0.1mm.

All specimens fractured by one single crack at the ligament. Fig. 2.11 and Fig. 2.12 shows the example photographs of the fibers across the crack during loading. Tensile stress is calculated by tensile load divided by sectional area at the ligament considering the specimen with notch. The relationships of tensile stress versus crack width (opening at the ligament) are shown in Fig. 2.13. The test results are summarized in Table 2.6. As the same as the aramid specimens without notch, a significant drop can be observed at first cracking and the second peak can be obtained from the experiment result. The average tensile stresses of aramid, PP and PVA specimens at the second peak are 3.02 MPa (crack width at 0.995mm), 1.61MPa (crack width at 1.199mm) and 1.80MPa (crack width at 0.680mm), respectively.

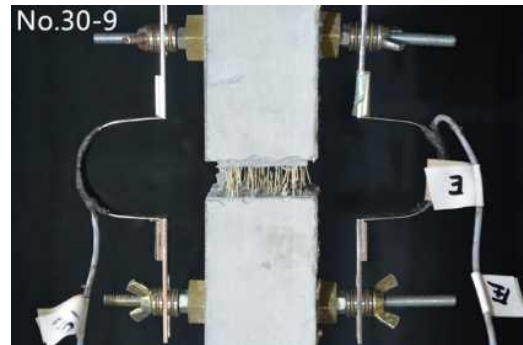
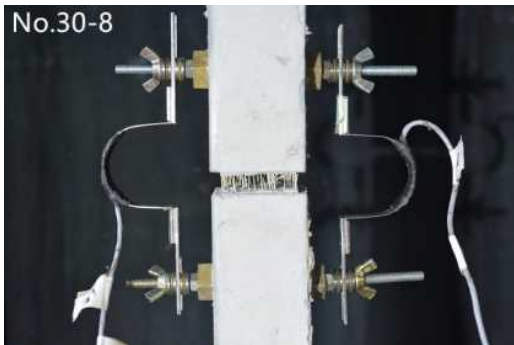
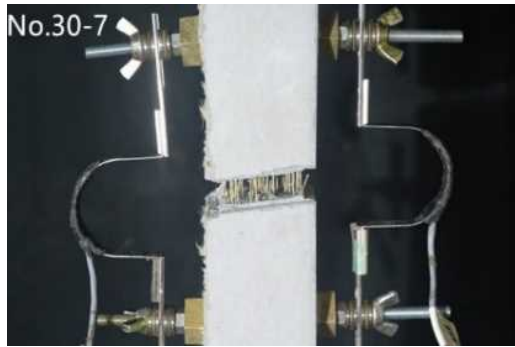


**Fig. 2. 11** Fibers across the crack during loading aramid specimens

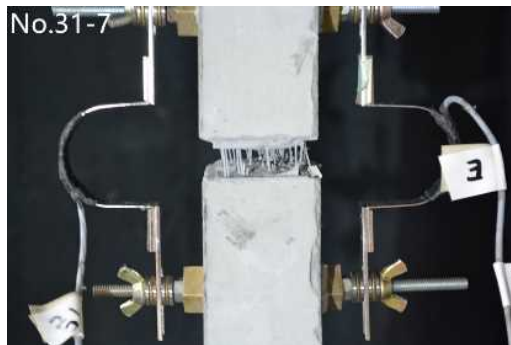
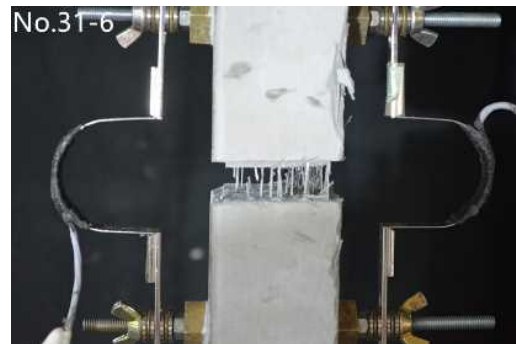
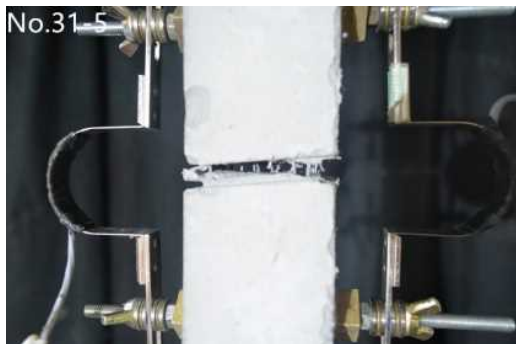


**Fig. 2. 12** Fibers across the crack during loading of PP specimens

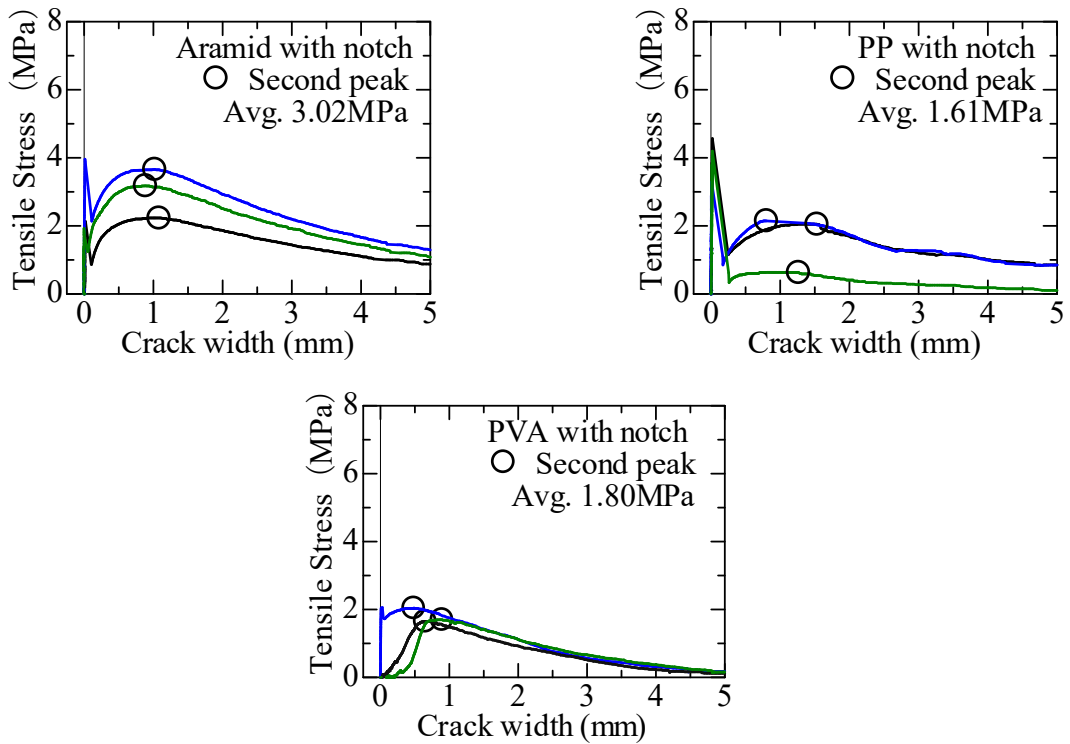


Fig. 2. 13 Tensile stress-crack with curve

Table 2. 6 Tensile test results specimens with notch

ID		At first cracking (first peak)		Maximum after cracking (second peak)	
		Tensile stress (MPa)	Crack width (mm)	Tensile stress (MPa)	Crack width (mm)
Aramid with notch	No.30-7	1.93	0.002	3.18	0.885
	No.30-8	2.13	0.019	2.23	1.081
	No.30-9	3.96	0.012	3.66	1.020
	Average	2.67	0.011	3.02	0.995
PP with notch	No.31-5	4.20	0.020	0.63	1.264
	No.31-6	4.57	0.021	2.05	1.531
	No.31-7	3.34	0.274	2.15	0.802
	Average	4.03	0.11	1.61	1.20

The final condition of cross section are shown in the Fig. 2.14 and Fig. 2.15. The bridging fibers across the section were counted after loading. The total numbers of fiber from up side and bottom side are listed in Table 2.7. The calculated total number of fibers using Eq (2.1) for aramid and

PP specimens with notch is 81.5 and 41.6. Aramid specimens showed the same tendency with the specimen without notch as that the counted total number of fibers was more than calculated value.

The total number of fibers for specimen No.30-7, No.30-8 and No.30-9 are 95, 76 and 143 which leads to No.30-9 has the highest tensile strength and No. 8 has the lowest tensile strength among the aramid specimens. The total number of fibers for specimen No.31-5, No.31-6 and No.31-7 are 27, 50 and 54 which results in No.31-5 has the lowest tensile strength. No.31-6 and No.31-7 have almost the same number of fibers which results in a same tendency of tensile strength.



**Fig. 2. 14 Final condition of cross section of aramid specimens**

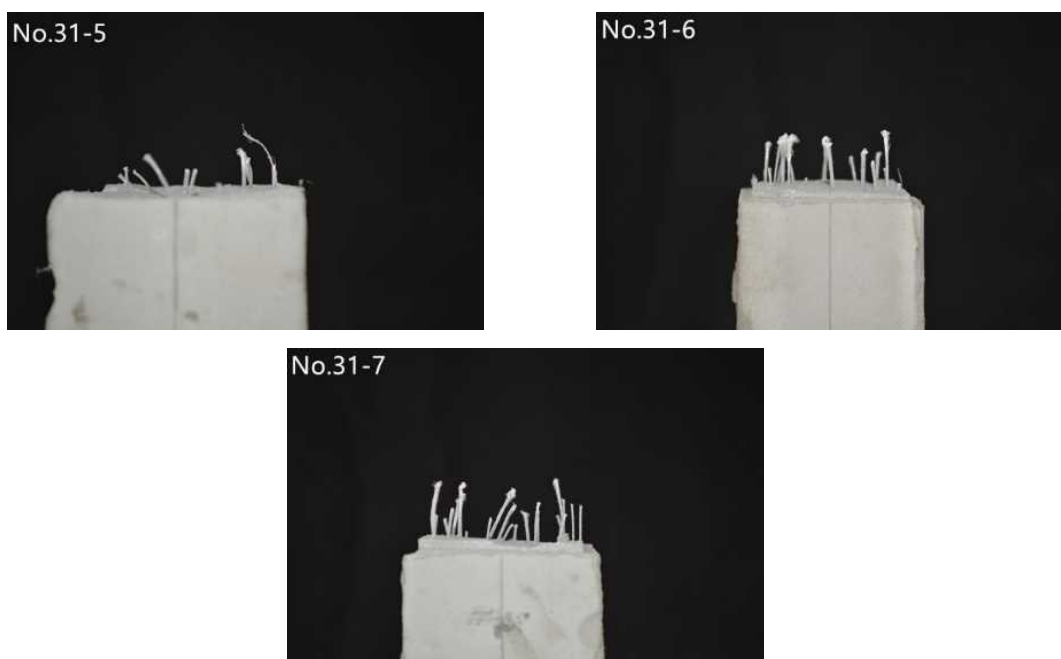


**Fig. 2. 15 Final condition of cross section of PP specimens**

**Table 2. 7 Counted total number of fibers across section of specimens with notch**

ID		Numbers of fiber across section					
		Up side		Bottom side		Total (Up+Bottom)	
		Of each	Average	Of each	Average	Of each	Average
Aramid with notch	No.30-7	49	54.7	46	50.0	95	104.7
	No.30-8	39		37		76	
	No.30-9	76		67		143	
PP with notch	No.31-5	12	20.3	15	23.3	27	43.7
	No.31-6	22		28		50	
	No.31-7	27		27		54	

Although both the results of unnotched specimens and notched specimens could express the tensile behavior of FRCC, however the relationship of tensile stress and crack width could not be measured from the experiment directly due to the influence of multiple cracks. Since only one single crack was occurred in the case of notched specimens, the relationship of tensile stress and crack width was obtained more precisely comparing to the specimens without notch.

## 2.3 Bending Test

### 2.3.1 Outline of experiment

The bending test was conducted for the same FRCCs used in uniaxial tension test. The specimens are divided into two series, i.e., three-point bending test with notched specimen and four-point bending test without notch.

### 2.3.2 Three-point bending test

#### 2.3.2.1 Test specimens and loading method

The notched beam specimens with 100mm square section (as shown in Fig. 2.16) specified in JCI-S-002-2003 [2.8] were used. As shown in Fig. 2.17, the notch was cut in the middle of specimen with a depth of 30mm. One LVDT was set to measure the load point deflection (LPD).

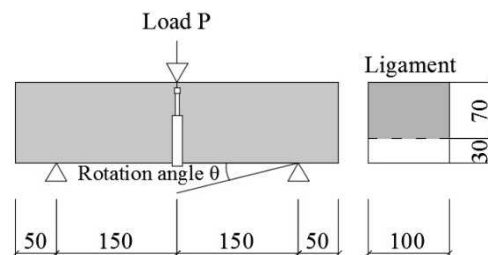


**Fig. 2. 16 Three-point bending test**

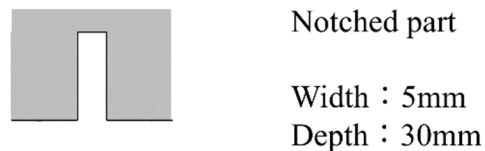


**Fig. 2. 17 Notched part of three-point bending test**

#### 2.3.2.2 Experimental results and discussion

The failure patterns of three-point bending specimens are shown in Fig. 2.18 and Fig. 2.19. All specimens fractured by only one single crack at the ligament. For three-point bending test specimen, the rotation angle is defined as load point deflection (LPD) divided by half of span (150mm). In order to compare the difference of specimens with or without notch, the bending stress is also defined as bending moment at the load point divided by section modulus. The relationships of bending stress and rotation angle for aramid and PP specimens are shown in Fig. 2.20. In case of aramid specimens, the load was increased significantly after first cracking to maximum. For PP specimens, the load dropped after the maximum load and increased gradually again showing second peak load. The average of bending stresses at the maximum load after the

sudden drop of the load (second peak) is 4.37 MPa and 2.13 MPa for aramid three-point and PP three-point specimen.

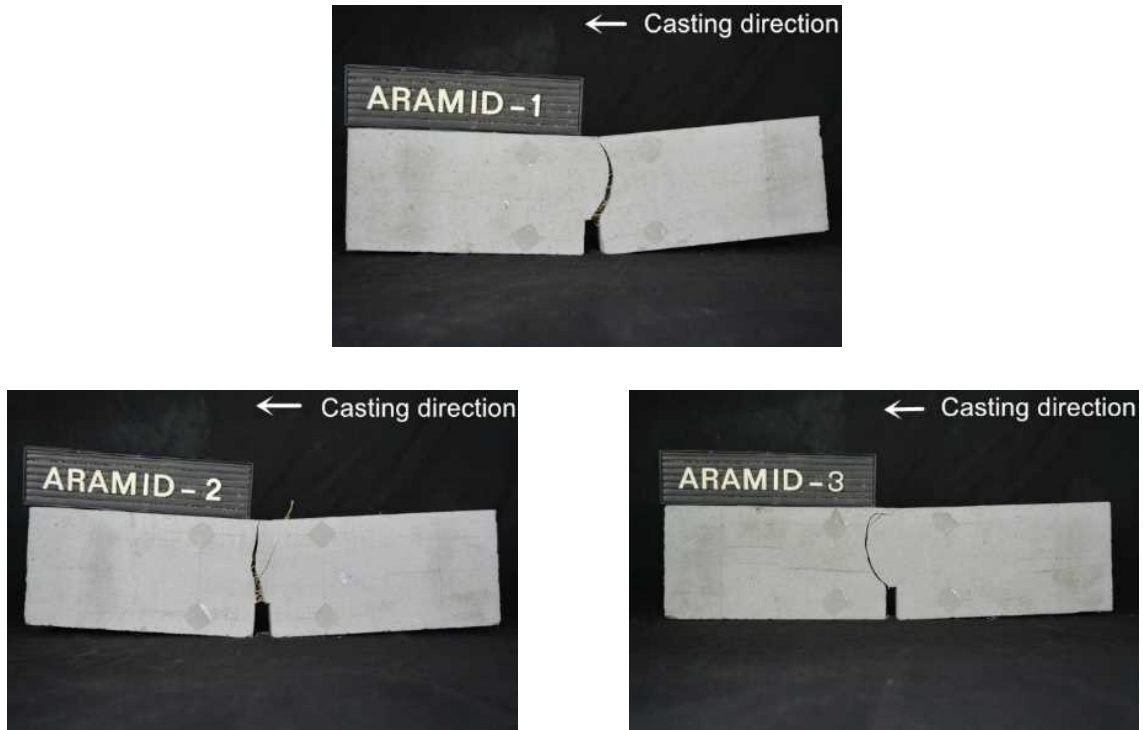


**Fig. 2. 18 Failure patterns of aramid specimens**

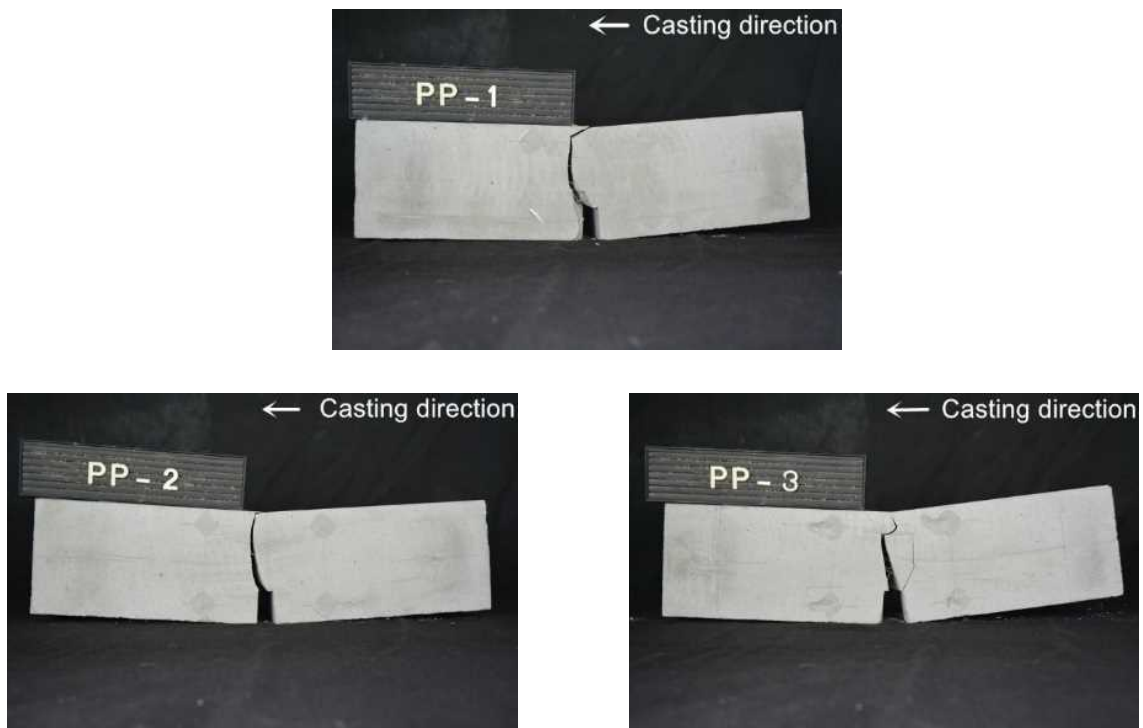


**Fig. 2. 19 Failure patterns of PP specimens**

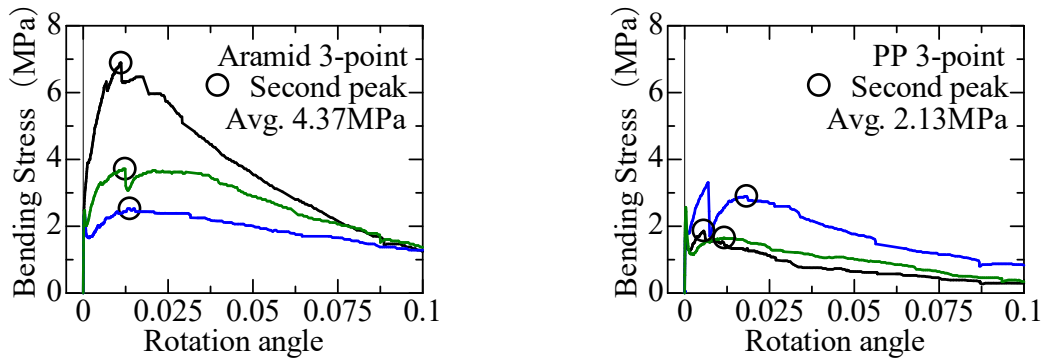


**Fig. 2. 20 Bending stress – rotation angle curve**

### 2.3.3 Four-point bending test

#### 2.3.3.1 Test specimens and loading method

The four-point bending test (as shown in Fig. 2.21) based on JCI-S-003-2007 [2.9] was carried out. Three LVDTs were set to measure the load point deflections (D1, D2) and the deflection at the center of the specimen.

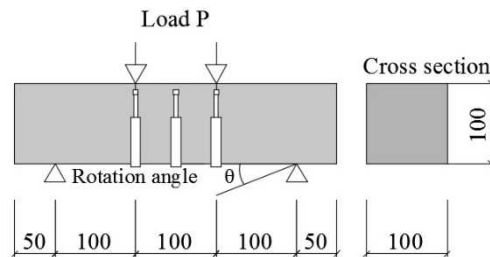


**Fig. 2. 21 Four-point bending test**

#### 2.3.3.2 Experimental results and discussion

In case of four-point bending test specimen, the rotation angle is defined as the average of load point deflections (D1, D2) divided by shear span (100mm). The bending stress is also defined as bending moment at the load point divided by section modulus. The failure patterns of four-point bending test are shown in Fig. 2.22 and Fig. 2.23. The relationships of bending stress and rotation angle for aramid and PP specimens are shown in Fig. 2.24. As same as three-point bending test, the load of aramid four-point specimens was increased significantly after first cracking to maximum and then decreased gradually. For PP specimens, the load dropped after the maximum load and increased gradually again showing second peak load. The average of bending stresses at the maximum load after the sudden drop of the load (second peak) is 5.48 MPa and 2.44 MPa for aramid four-point and PP four-point specimen.

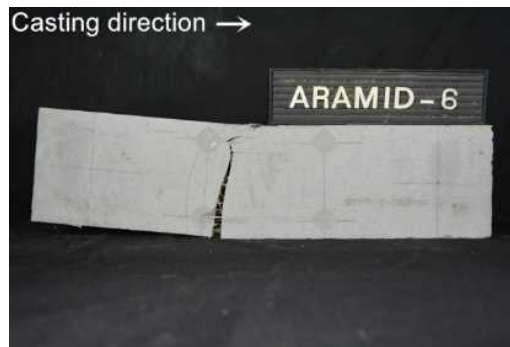
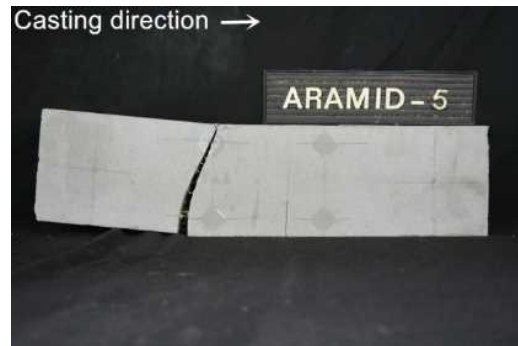
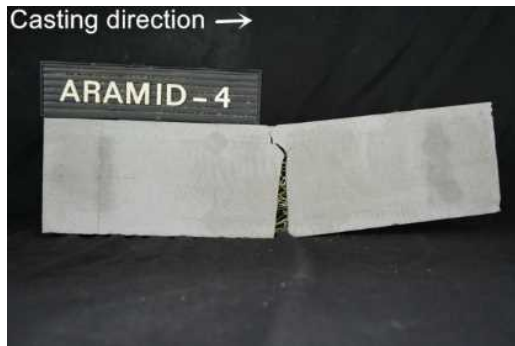


**Fig. 2. 22 Failure patterns of aramid specimens**

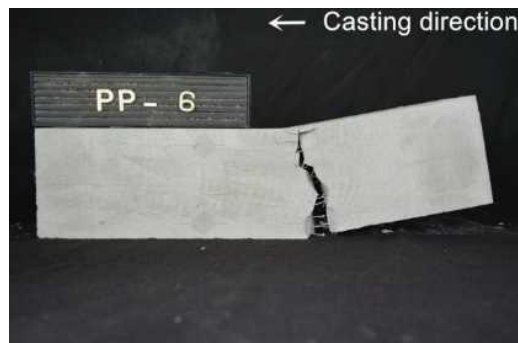
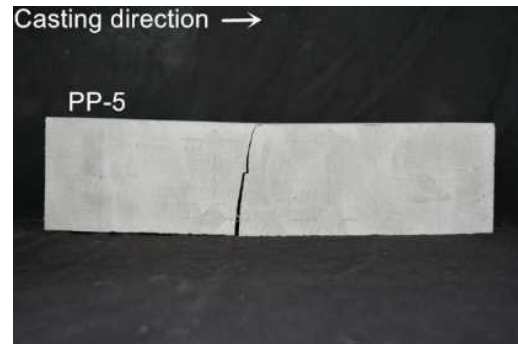
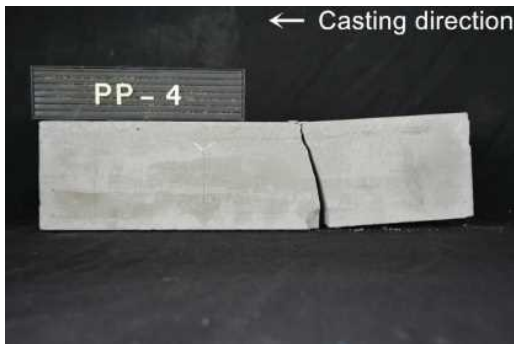


**Fig. 2. 23 Failure patterns of PP specimens**

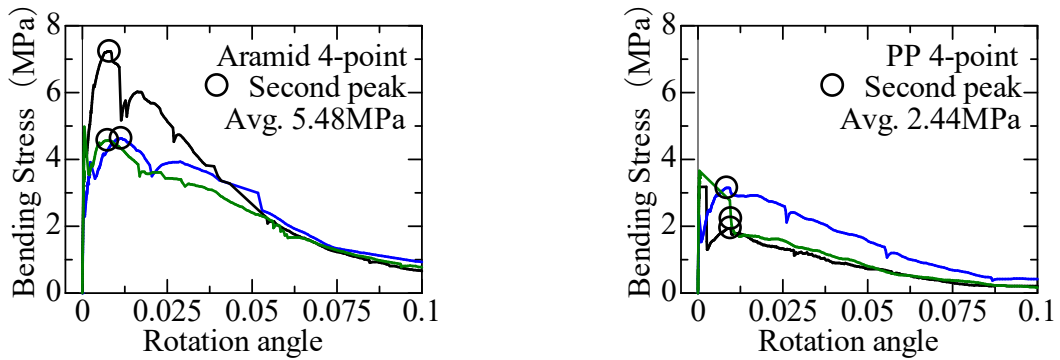


**Fig. 2. 24 Bending stress – rotation angle curve**

The results of unnotched specimens and notched specimens indicated that both three-point bending test and four-point bending test could describe the flexural performance of FRCC. The notch on bending test specimen does not largely affect the peak stress after first cracking.

#### 2.4 Conclusions

The tensile and flexural behavior of FRCC has been confirmed from uniaxial tension test and bending test directly by specimens with or without notch.

Since only one single crack was occurred in the case of notched specimens of uniaxial tension test, the relationship of tensile stress and crack width was evaluated more accurately by the result obtained from the experiment directly. The maximum tensile stresses of specimens with notch for PVA, aramid and PP specimens are 1.80 MPa, 3.02 MPa and 1.61 MPa which could be used to evaluate the structural performance of FRCC.

Both three-point bending test and four-point bending test could represent the flexural behavior of FRCC and only one single crack was observed during loading for two types of bending specimen. The notch on bending test specimen nor uniaxial tension test specimen does not largely affect the peak stress after first cracking in case of FRCCs tested in this study.

## CHAPTER 3 Influence of Fiber Types on Structural Performance of FRCC Beam-Column Joints

### 3.1 Introduction

Beam-Column Joint is the crucial part of a RC frame, which is to ensure the ductility of the whole structure especially when the frame is subjected to huge earthquake. Major damage should be avoided in the beam-column joint. Even the beam and column step into inelastic state, the joint has to remain the ability to transfer actions. With the development of society, new materials are demanded to reinforce the new modern buildings. Comparing to the conventional concrete, FRCC has a remarkable deformability especially under tensile and bending loading with large energy absorption capacity due to the effect of fiber bridging is expected to be used in the crucial part of a RC frame to improve the structural performance. However, due to the difficulties to keep flowability, avoiding fiber clustering during casting and high cost, it could be only used in the panel zone of beam-column joint. Separated casting of panel zone from beam and column is required for making of FRCC beam-column joint (Fig. 3.1). Such difficulties limit the utilization of FRCC into a real RC frame.



**Fig. 3. 1 Casting separately**

Precast (PCa) construction method which is used in reinforced concrete buildings especially in high skyscraper becomes more popular by ensuring good quality, simplified install procedure and shorter duration. As shown in Fig. 3.2, the main idea of this precast system is to cast the joint panel combined with the beam and separate the column into counterparts [3.1]. By manufacturing in factory, PCa construction method could ensure FRCC to play a better role in the panel zone of beam-column joint to improve the structural performance.

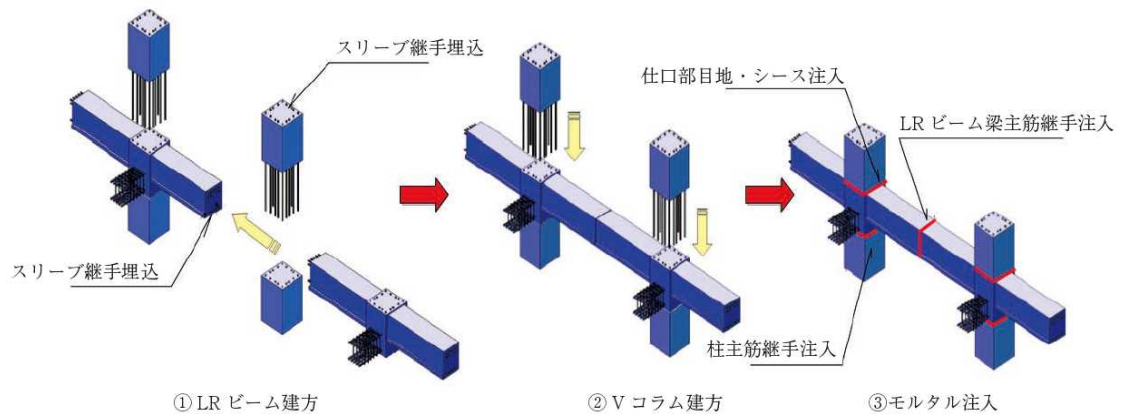


**Fig. 3. 2 LRV-Precast System [3.1]**

With the development of polymer material, various synthetic polymer fibers have become the best selection to improve concrete capacity and failure resistance without corrosion of fibers. The influence of fiber types on tensile and bending performance of FRCC has been confirmed in Chapter 2. In this Chapter, aramid and PP fibers were used as 1% volume fraction in panel zone to seek the influence of fiber types on structural performance of FRCC beam-column joint. The results of beam-column joint without fiber and beam-column joint using PVA FRCC are also included to compare with aramid and PP FRCC beam-column joints.

## 3.2 Experimental Program

### 3.2.1 Specimens

Assuming from the middle to upper floors of high-rise RC buildings by full precast construction method, two beam-column joint specimens (No.30 and No. 31) were designed to fail by shear in panel zone before flexural yielding to evaluate the shear performance of joint panel. FRCCs were only used in the panel zone. Dimensions of the FRCC beam-column joints are shown in Fig. 3.3 and Table 3.1. The column section was 500 mm × 500 mm and the beam section was 380mm wide and 420mm deep. The span of beam and column was 2700 mm and 1560 mm which is considered as a half scale of real RC structure. High strength rebars were adopted for main reinforcing bars in beam and column to insure the priority of shear failure in panel zone. To grasp the fiber influence on the shear performance of panel zone, no hoop was used in panel zone.

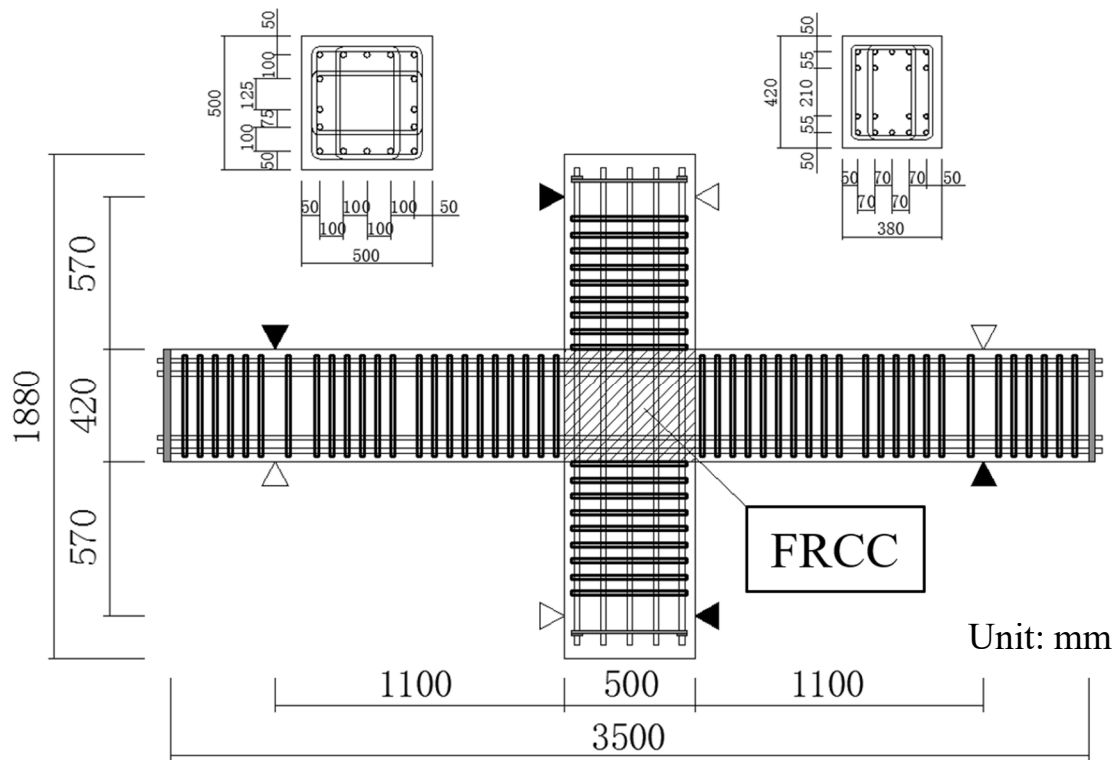


**Fig. 3. 3 Specimen dimensions**

**Table 3. 1 Specimens list**

ID	Panel	Beam		Column	
	Parameter	Reinforcing bar	Stirrup	Reinforcing bar	Hoop
No.24*	Without fiber	18-D22 (USD685)	6-D10@60 (SD785)	16-D22 (USD685)	6-D10@60 (SD785)
No.25*	PVA				
No.30	Aramid				
No.31	PP				

\*Specimen No.24, No.25 are from the previous study (Sano et al., 2015) [3.2]

In order to compare FRCC beam-column joints shear performance better, specimens from the previous study [3.2] is also listed in this study. The authors have reported the experimental results of No. 24 (without fiber) and No. 25 which is the specimen has 1% PVA fiber in panel zone. All other parameters are same as this research.

For simplifying the procedure of making specimens, the mechanical connections and grouted mechanical sleeves have not been used in the fabrication. First, a foundation for the mold was prepared as shown in Fig. 3.4. Second, bar arrangement and the mold for panel zone were made

as shown in Fig. 3.5. Third, casting the panel zone using FRCC was done as shown in Fig. 3.6. Fourth, demolding the mold of panel zone as shown in Fig. 3.7 and then install lateral reinforcements and molds for beam and column were made as shown in Fig. 3.8. Last, conventional concrete was casted in the beam and column as shown in Fig. 3.9.



**Fig. 3. 4 Foundation platform**



**Fig. 3. 5 Mold for panel zone**



**Fig. 3. 6 Casting the panel zone**



**Fig. 3. 7 Demolding**



**Fig. 3. 8 Install lateral reinforcements and the molds**



**Fig. 3. 9 Casting beam and column**

### 3.2.2 Materials properties

FRCC used in beam-column joint test is as same as the materials used in tensile and bending test which has been introduced in Chapter 2. The fiber volume fraction was set to 1% for all specimens. The mechanical properties of FRCC used in joint core region are listed in Table 3.2.

**Table 3. 2 Mechanical properties of FRCC**

ID	Parameter	Place	Compressive strength (MPa)	Elastic modulus (GPa)
No.24*	Without fiber	Joint core region	50.3	17.6
No.25*	PVA		52.5	17.1
No.30	Aramid		51.3	17.7
No.31	PP		51.5	17.2

\*Specimen No.24, No.25 are from the previous study (Sano et al., 2015) [3.2]

Conventional concrete was used in the column and beam parts of the specimen. The compression test and splitting test were carried out with the cylinder test pieces ( $\phi 100$  mm x 200 mm). In The mixture proportion of concrete is listed in Table 3.3 and the mechanical properties of concrete are listed in Table 3.4.

**Table 3. 3 Mixture proportion of concrete used for beam and column**

ID	Parameter	Place	Target Strength (MPa)	Unit weight (kg/m <sup>3</sup> )				
				Water	Cement	Fine aggregate	Coarse aggregate	Admixture
No.24*	Without fiber	Beam	36	170	378	833	910	3.78
No.25*	PVA							
No.30	Aramid	Column	68	175	593	746	867	7.41
No.31	PP							

\*Specimen No.24, No.25 are from the previous study (Sano et al., 2015) [3.2]

**Table 3. 4 Mechanical properties of concrete**

ID	Parameter	Place	Compressive strength (MPa)	Splitting tensile strength (MPa)	Elastic modulus (GPa)
No.24*	Without fiber	Beam	39.9	3.55	29.6
No.25*	PVA		39.1	3.42	28.0
No.30	Aramid	Column	83.4	4.09	37.1
No.31	PP		72.8	4.15	38.0

\*Specimen No.24, No.25 are from the previous study (Sano et al., 2015) [3.2]

To prevent the flexural failure of beam, high strength rebars were adopted for main reinforcing bars in beam and column. The mechanical properties of reinforcing bars and hoops are listed in

Table 3.5. The nominal cross-section area was adopted for the calculation of yield strength, tensile strength and elastic modulus.

**Table 3. 5 Mechanical properties of rebars**

Type	Diameter	Place	Yield strength (MPa)	Tensile strength (MPa)	Elastic modulus (GPa)
USB685	D22 (22 mm)	Longitudinal reinforcing bar	717	900	195
SD785	D10 (10 mm)	Stirrup Hoop	832	996	218

### 3.2.3 Loading and measurement

The reversed cyclic loading is applied to the beams by controlling story drift angles  $R=\pm 1/400$ ,  $\pm 1/200$ ,  $\pm 1/100$ ,  $\pm 1/67$ ,  $\pm 1/50$ ,  $\pm 1/33$ ,  $\pm 1/25$ ,  $\pm 1/20$  and  $+1/14$  rad. Story drift angle was controlled by the actuators attached to the inflection points of beams which is shown in Fig. 3.10. Oil jacks were used on the inflection points to support the columns. The axial force ratio was set to 0.05 which was applied on the column manually. The measurements were the applied load on beams, story drift angle, deformations of beam and column. Setups of linear variable displacement transducers (LVDTs) are shown in Fig. 3.11 and Fig. 3.12.

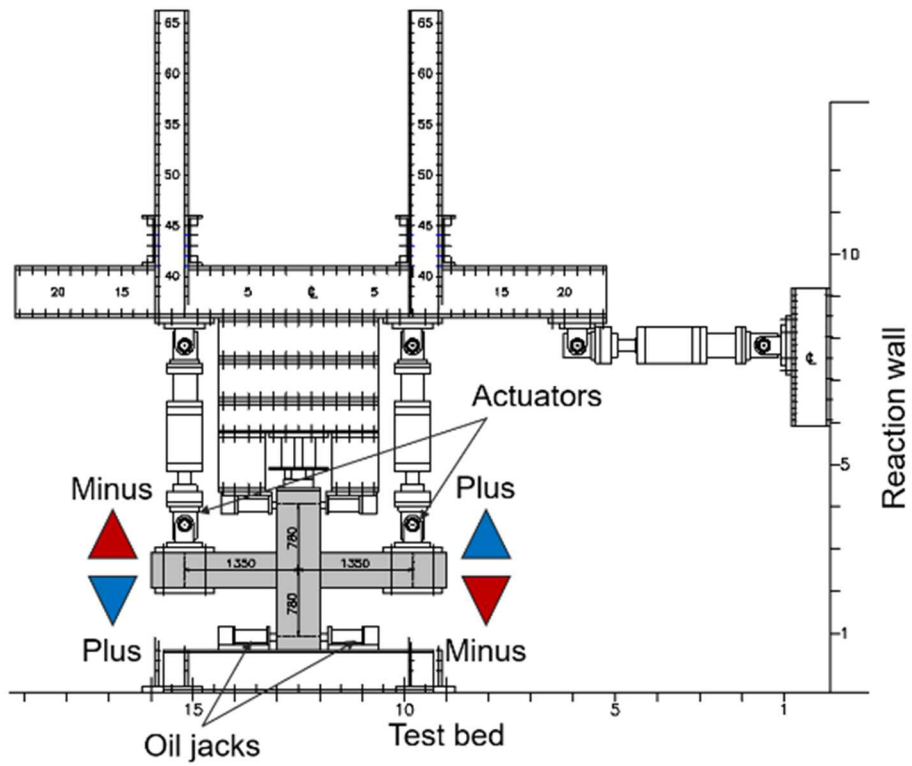


Fig. 3. 10 Loading method

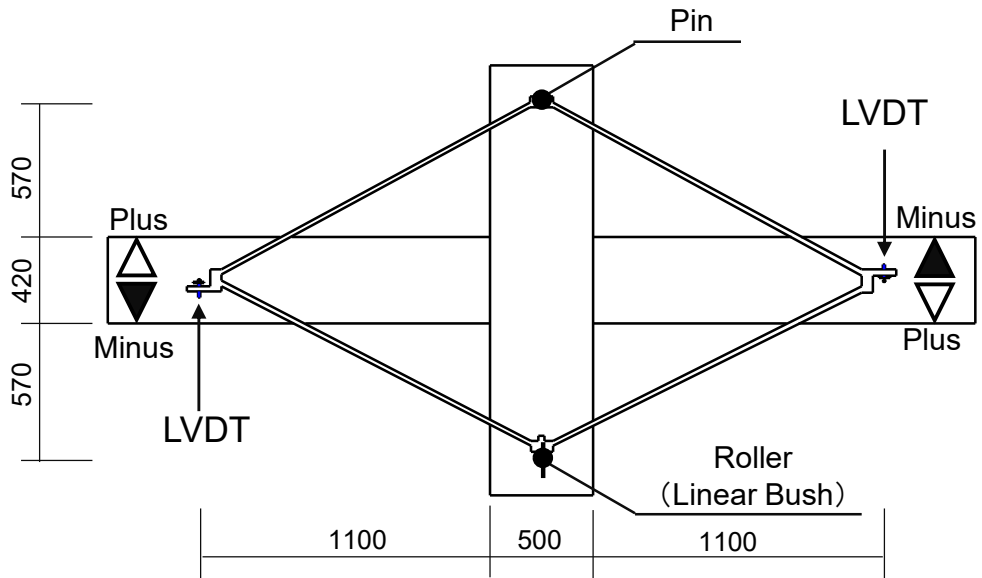
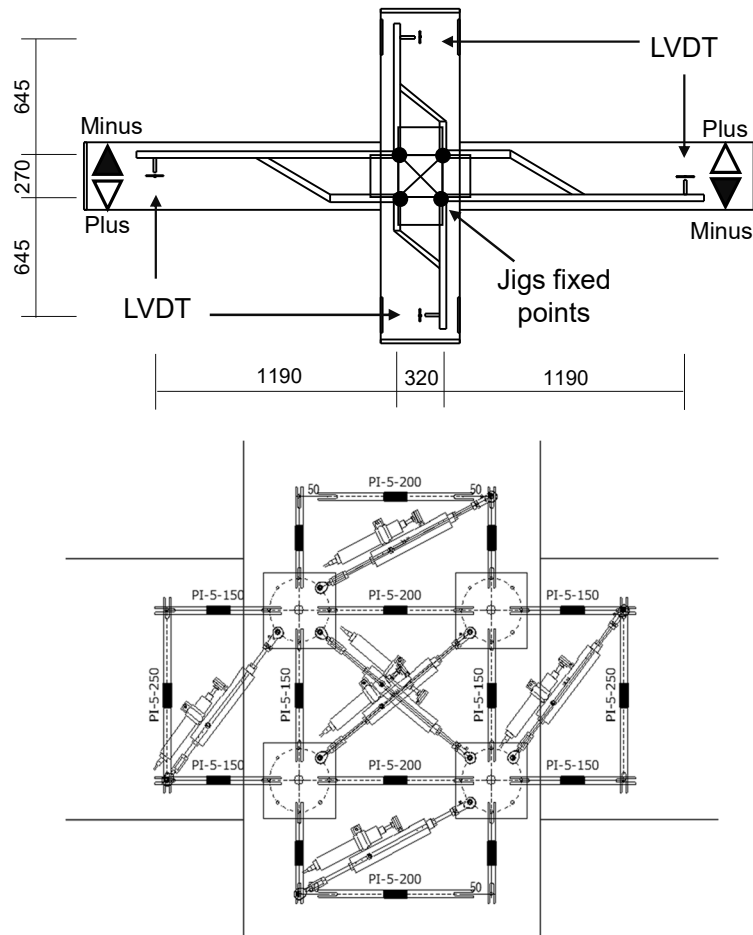


Fig. 3. 11 Measurement of story drift angle



**Fig. 3. 12 Measurement of local deformation**

### 3.2.4 Experimental results

#### 3.2.4.1 Failure modes

Crack patterns of all specimens observed at maximum load are shown in Fig. 3.13. Except for No.30, maximum loads of all specimens were observed at story drift angle  $R=1/50\text{rad}$ . Due to aramid fiber has a higher fiber bridging effect, maximum load of No. 30 was observed at story drift angle  $R=1/33\text{rad}$ . The failure in strut mechanism of No. 30 was observed at story drift angle  $R=1/33\text{rad}$ . of which  $R=1/50\text{rad}$ . for No. 31 specimen. For all specimens, shear crack occurred on panel zone first, then flexural crack and shear crack on beams were observed in this order. Diagonal shear crack on panel zone developed more and more visible due to crack opening and closing under the increased cyclic load. Large number of diagonal cracks appeared on the surface of panel zone during loading which leads to the shear failure. In comparison with No. 24, the cracks of all specimens with fibers have been inhibited due to the effect of fiber bridging. After maximum load, the cracks of specimens with fibers developed wider and deeper, however if compared to No. 24, the change was not obvious. By using fibers into beam-column joint, the

damage of panel zone can be improved.



No. 24 (No fiber) \*  $R=1/50$  rad.



No. 25 (PVA) \*  $R=1/50$  rad.



No.30 (aramid)  $R=1/33$  rad.



No. 31 (PP)  $R=1/50$  rad.

**Fig. 3. 13 Failure patterns**

\*Specimen No.24, No.25 are from the previous study (Sano et al., 2015) [3.2]

#### 3.2.4.2 Crack patterns and crack width

To observe the shear crack patterns and crack width of beam-column joint, photos of the surface of joint core region were taken during loading by two cameras which were installed in front to the specimen. Due to shear diagonal cracks were expected to be occurred in the middle of joint panel, the target photographing region was set as shown in Fig. 3.14.

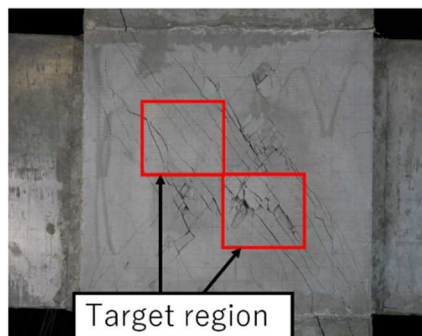


**Fig. 3. 14 Photographing region**

As shown in Fig. 3.15, meshes of 10 mm × 10 mm were drawn on the target photographing region before loading. To grasp the transition of crack properties which changed with deformation, the photographing region was set as 120 mm × 80 mm by considering 1 pixel is equivalent to 0.02 mm. The shooting interval was set to every 10 seconds by considering the loading speed.

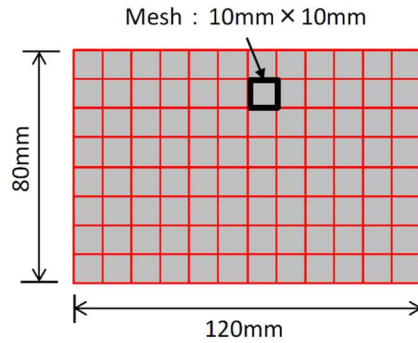


**Fig. 3. 15 Details of photographing region**

The photos of peak of each loading cycles are shown in Fig. 3.16-Fig. 3.18. The results in Fig. 3.16 are from the previous research [3.2]. The widest crack is pointed out by the red arrows in each photo. by analyzing the widest crack occurred in each loading cycles.

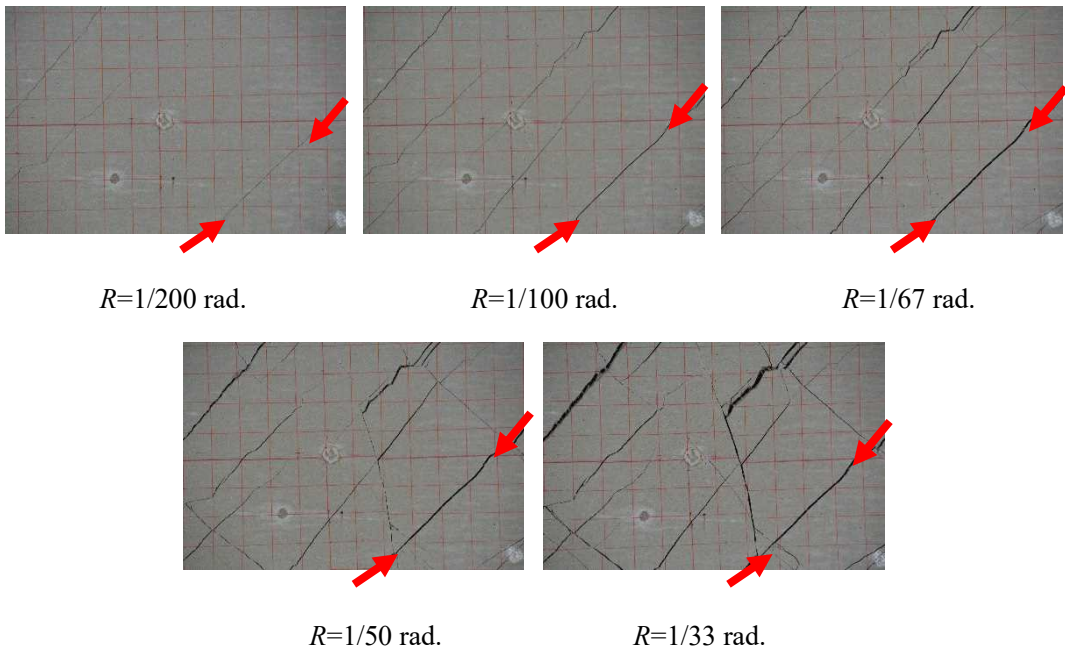


**Fig. 3. 16 Crack patterns of No.25 (PVA)\***

\*Specimen No.25 is from the previous study (Sano et al., 2015) [3.2]

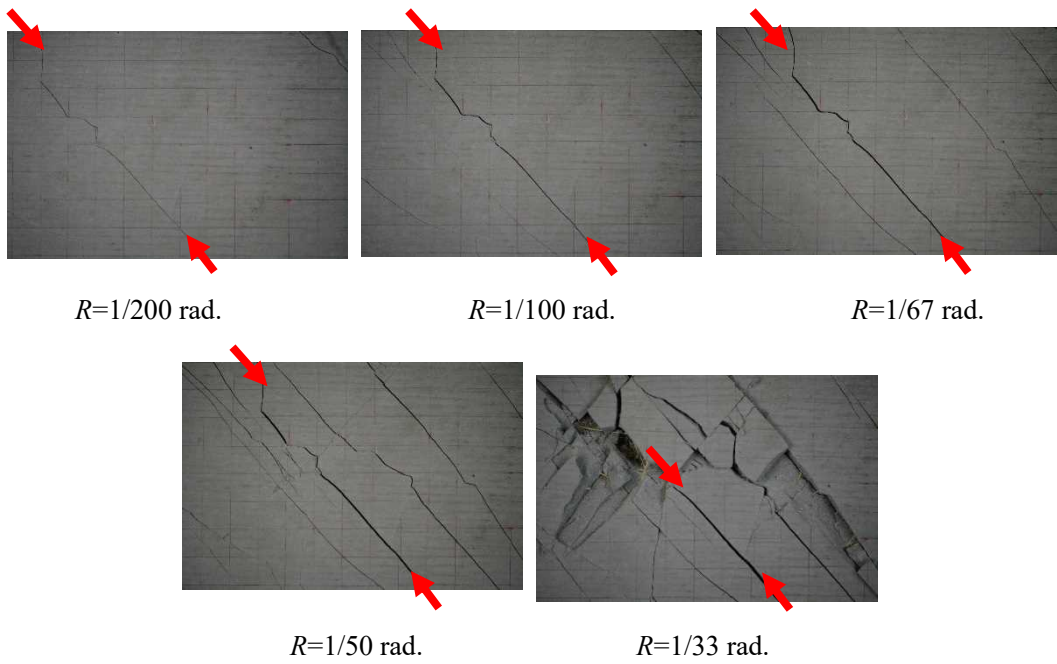


**Fig. 3. 17 Crack patterns of No.30 (aramid)**

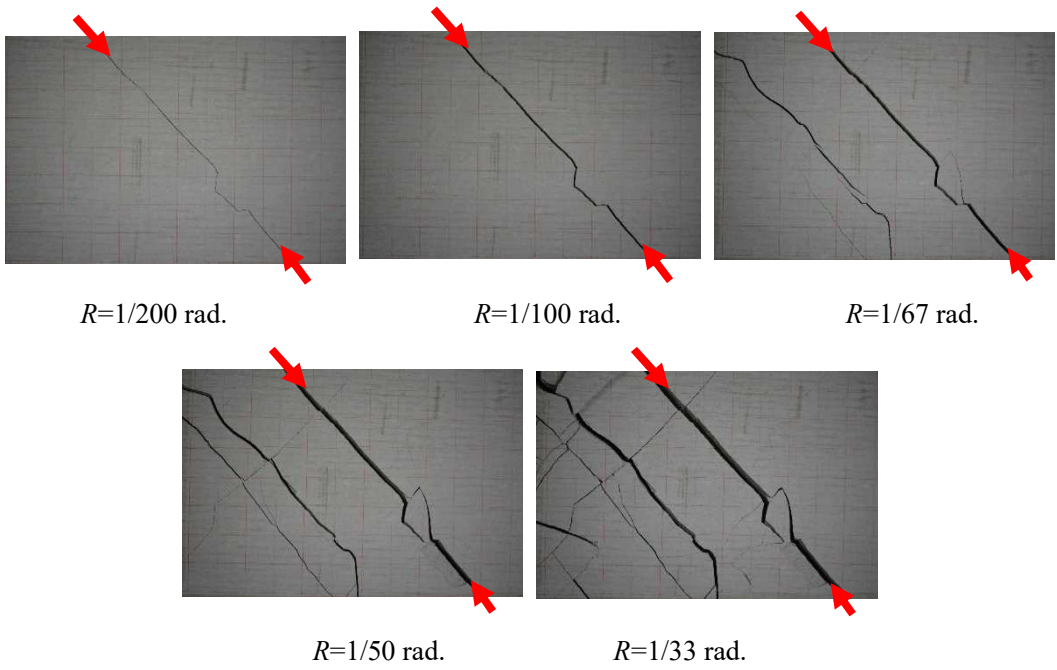


**Fig. 3. 18 Crack patterns of No.31 (PP)**

The evaluation method of crack properties is shown in Fig. 3.19. It is considered that the shear crack surface generated in the panel zone is under a biaxial stress state where tensile stress and shear stress act simultaneously. Therefore, the crack opening is defined as the displacement in the direction perpendicular to the crack due to the action of tensile stress. The displacement in the

direction along the crack due to the action of shear stress is defined as crack sliding. The displacement in the principal stress direction by considering the crack opening and crack sliding is defines as crack width. From the photo, the crack opening, sliding and width at each intersection could be evaluated by the coordinates generated by the meshes.

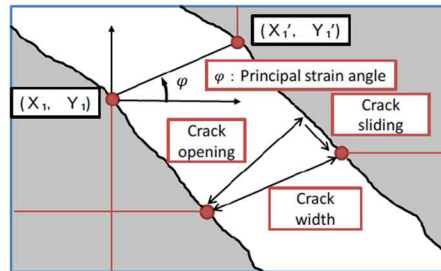


**Fig. 3. 19 Evaluation of crack properties**

The calculated crack width of specimen No. 30 and No. 31 are shown in Fig. 3.20. In all specimens, the crack width increased as the panel zone deformation progressed and the residual crack width increased with the increment of each cycle.

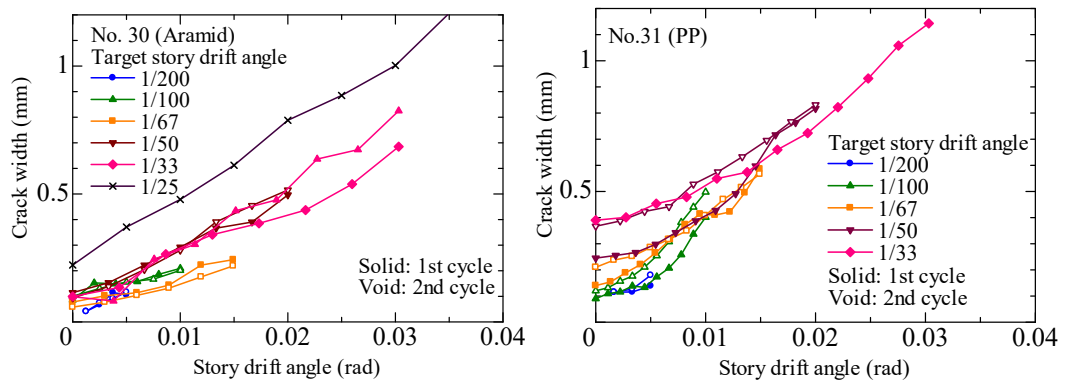


**Fig. 3. 20 Crack width**

The calculated crack opening of specimen No. 30 and No. 31 are shown in Fig. 3.21. All specimens showed similar tendency to crack width, the crack opening increased as the panel zone deformation progressed and the residual crack width increased with the increment of each cycle. The calculated results of crack sliding are shown in Fig. 3.22.

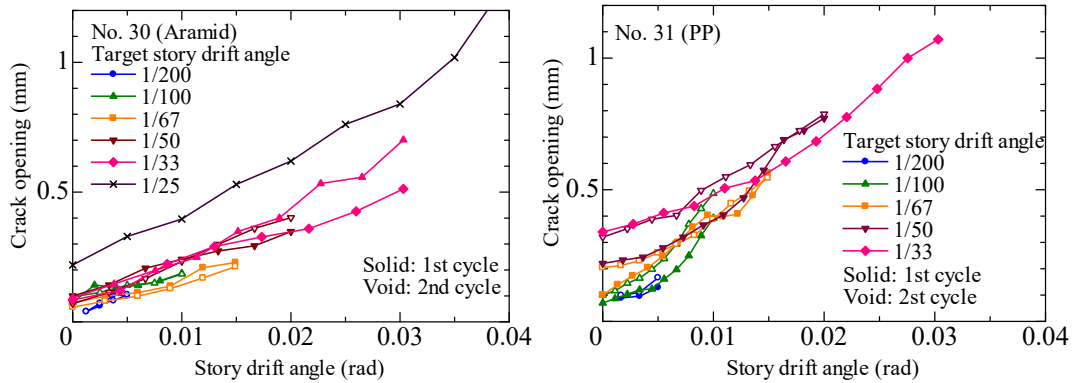


**Fig. 3. 21 Crack opening**

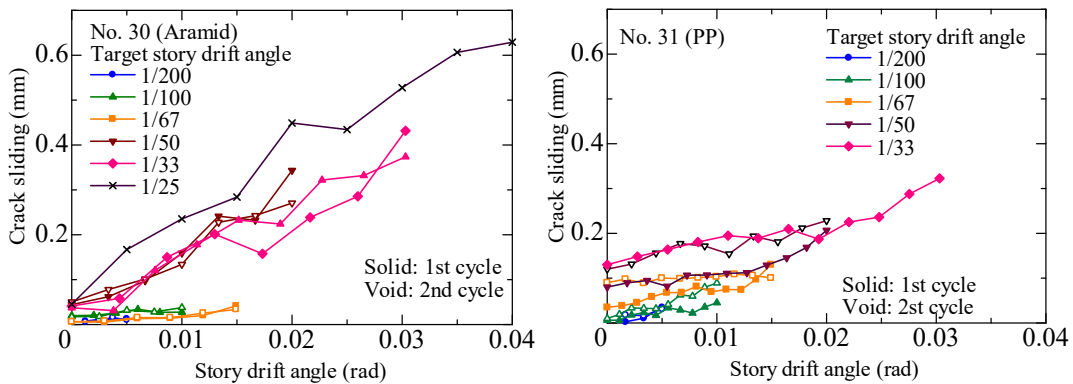


**Fig. 3. 22 Crack sliding**

Similarly, the principal strain angle and crack angle were also calculated by using the captured coordinates of the intersection of mesh and crack. Each point in the figure represents the principal strain angle or crack angle of the peak load of each loading cycle as shown in Fig. 3.23. The principal strain angle decreased with the increment of each loading cycle. Meanwhile, the crack angle was remained the same which was around 45 degrees.

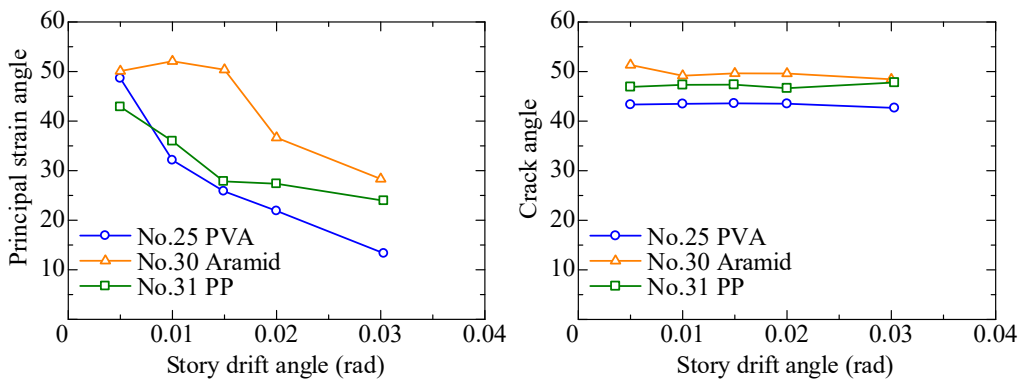


**Fig. 3. 23 Principal strain angle and crack angle**

\*Specimen No.25 is from the previous study (Sano et al., 2015) [3.2]

As shown in Fig. 3.24, the crack width, crack opening and crack sliding were also summarized as the value of the peak load of each loading cycle. The crack properties at the maximum load are summarized in Table 3.6.

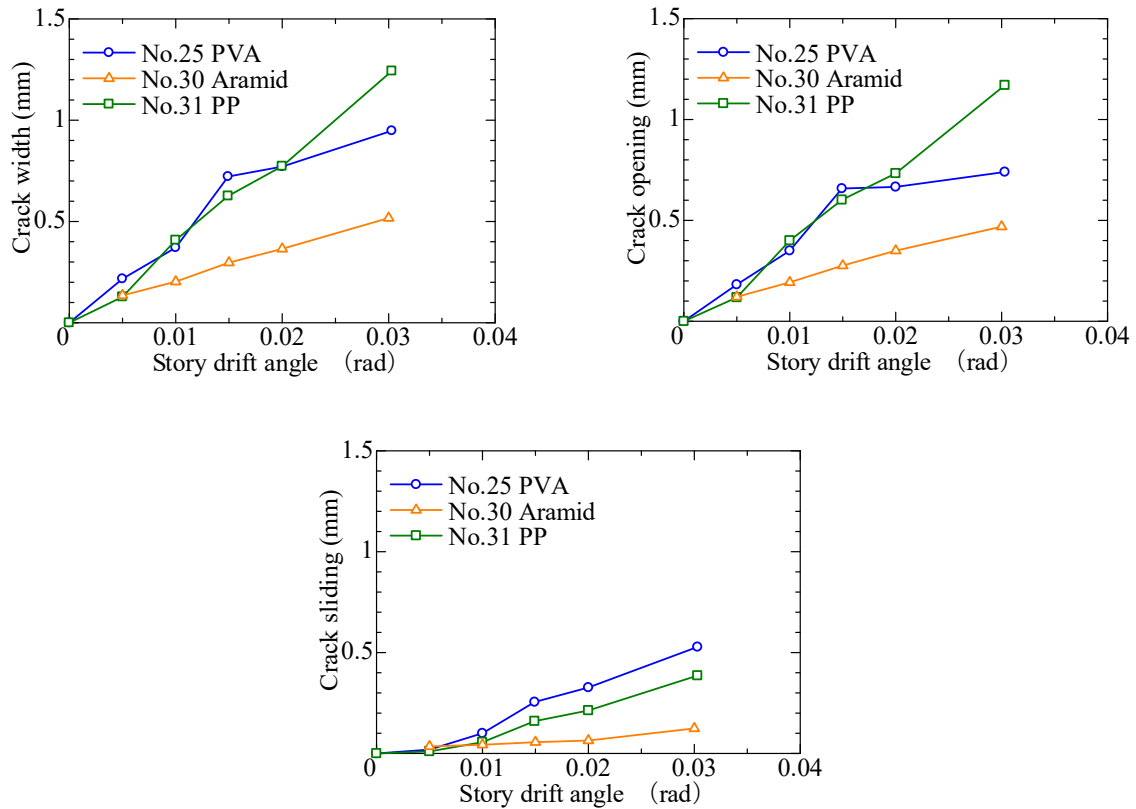


**Fig. 3. 24 Summary of crack opening, sliding and width**

\*Specimen No.25 is from the previous study (Sano et al., 2015) [3.2]

**Table 3. 6 Summary of crack properties at the maximum load**

ID	Cycle of maximum load	Crack width (mm)	Crack opening (mm)	Crack sliding (mm)	Principle strain angle (°)	Crack angle (°)
No. 25 PVA*	1/50 rad.	0.771	0.666	0.324	21.9	43.5
No.30 Aramid	1/33 rad.	0.517	0.469	0.124	28.3	48.4
No.31 PP	1/50 rad.	0.773	0.733	0.213	27.4	46.6

\*Specimen No.25 is from the previous study (Sano et al., 2015) [3.2]

For all specimens, the crack width increased with the increasing loading cycle. A better fiber bridging effect of aramid fiber was confirmed since the crack width of aramid specimen at maximum load is 0.517 mm which is about 70% of that in PVA and PP specimens. In the case of

PVA specimen, the crack width showed a slowing increasement after maximum load ( $R = 1/50\text{rad.}$ ) compared with PP specimen. It is considered PVA fiber has a better performance in inhibiting the crack width than PP fiber after maximum load.

The crack opening for all specimens had a same tendency with crack width. The crack opening increased with the increasement of loading cycle. Aramid specimen also showed a better ability in inhibiting the crack opening compared to PVA and PP specimen.

The crack sliding for PVA, aramid and PP specimens is 0.324 mm, 0.124 mm and 0.213 mm. The better characteristics of aramid specimen was also observed in inhibiting the deformation along the shear sliding direction. Comparing with crack width and crack opening, the small gradient of crack sliding results indicated that the crack sliding increased not obviously due to the effect of fiber bridging. However, after the loading cycle of maximum load, the crack sliding increased rapidly. At the same time the pull-out of fibers were observed obviously. It is considered that fibers resisted in the direction of shear force to the maximum load.

#### 3.2.4.3 Relationships of shear force and story drift angle

Fig. 3.25 shows the relationships of load and story drift angle obtained from the cyclic loading test. The maximum loads are listed in Table 3.7. Specimen No. 30 has the highest value of 544 kN, which was mainly attributed by its higher fiber bridging effect. Since all the specimens were designed by failure of panel zone, maximum load of specimens with fibers were increased significantly compared to No. 24 due to the effectiveness of fiber bridging.

**Table 3. 7 Maximum load and story drift angle at maximum load**

ID	Maximum load	Story drift angle
No.24 No fiber	389 kN	1/50 rad.
No. 25 PVA	443 kN	1/50 rad.
No.30 Aramid	544 kN	1/33 rad.
No.31 PP	495 kN	1/50 rad.

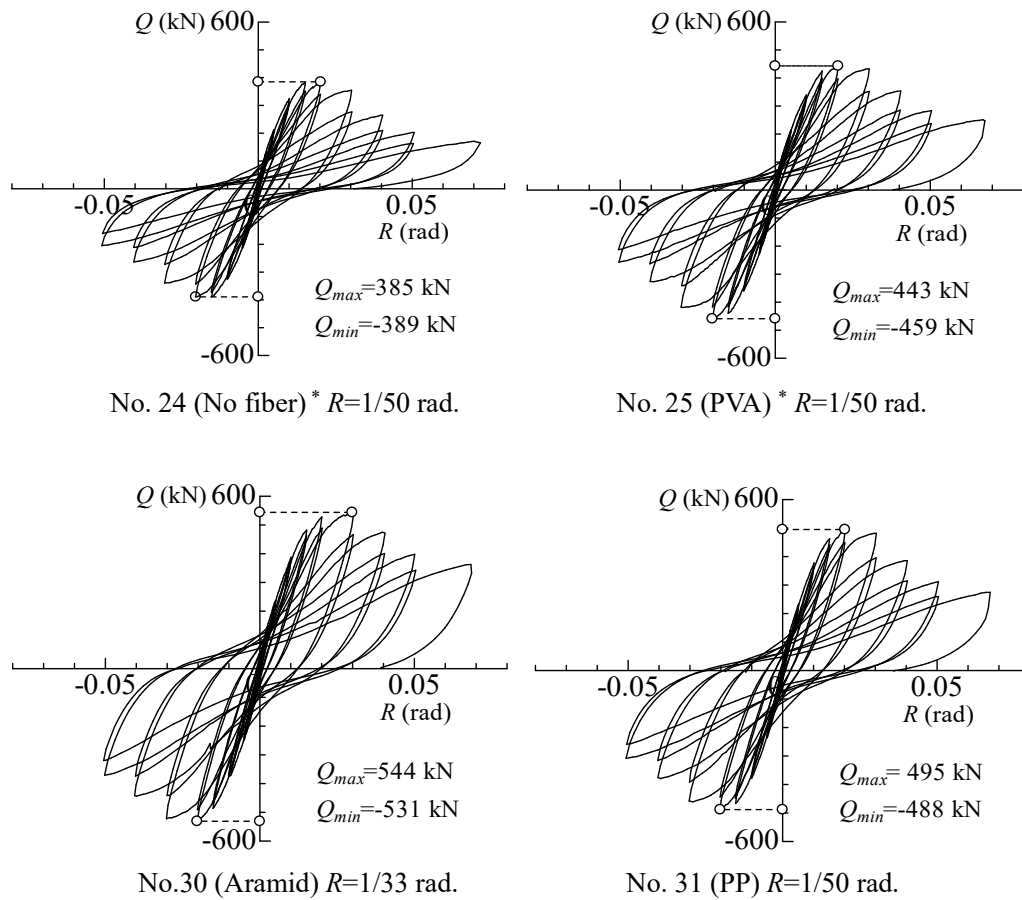


**Fig. 3. 25 Relationships of load and story drift angle**

\*Specimen No.24, No.25 are from the previous study (Sano et al., 2015) [3.2]

### 3.3 Conclusions

Comparing with specimen without fiber, the damage of specimens with fibers is inhibited due to the effect of fiber bridging. The maximum loads of beam-column joints increase by adding fiber. Specimen No.30 has the highest maximum load which is 544 kN. It is recognized that the bridging effect is different by types of fiber.

The observed crack width of diagonal shear crack was 0.771mm, 0.517mm, and 0.773mm for specimens with PVA, aramid and PP fiber at the condition of maximum load. Comparing with crack width and crack opening, the crack sliding increased not obviously. It is considered that fibers resisted in the direction of shear force.

## CHAPTER 4 Influence of Casting Method on Structural Performance of FRCC Beam-Column Joints

### 4.1 Introduction

FRCC used in this study has self-compacting characteristics with a high viscosity. It has been considered that fresh-state properties, casting method, vibration, flow and framework, etc. have the effect on the orientation of fibers [4.1]. When fibers tend to orient perpendicularly to crack surface, higher bridging effect of fibers is observed. When fibers tend to orient parallel to crack, however, bridging performance of fibers becomes poor. For tensile characteristics of FRCC, as one of the examples, the influence of casting direction on the tensile performance of FRCC has been studied through uniaxial tension test [4.2] and 2.1 times higher tensile stress of the second peak was observed in horizontal casting specimens than that of vertical casting specimens.

In this chapter, furthermore, a vibrator rod is used to reorient the fiber. Using a compacting vibrator shows an effectiveness to improve the bending behavior of FRCC [4.3]. Fig. 4.1 shows the example of visualization simulation using water glass solution conducted as like previous study [4.4]. The black-colored “target fibers” made from nylon were added to the matrix to ease the observation of fiber orientation. The cross-sectional size of the mold is 180mm x 280mm. The right-side photo shows the upper surface of the matrix after vibration using a compacting vibrator. It can be clearly observed that the fibers orient along concentric circles centering the point of vibrating. In this study, a vibrator rod is inserted into the matrix along with the direction of casting to arrange the fiber orientation of panel zone. The influence of using a vibrator rod during casting is also discussed based on the experimental results.



**Fig. 4. 1 Example of fiber orientation after vibrating [4.4]**

To clarify the influence of fiber orientation on structural performance of PVA FRCC beam-column joint by using two types of casting method, horizontal and vertical casting beam-column

joint specimens are tested by reversed cyclic load. A vibrator rod is also applied during the casting.

PVA fiber is used for all specimens with a fiber volume fraction of 1%. The dimensions of specimens and loading method are as same as mentioned in Chapter 3.

## 4.2 Experimental Program

### 4.2.1 Specimens and materials properties

The dimension of specimens has already presented in Fig. 3.5. PVA fiber is used for all specimens with a fiber volume fraction of 1%. Two types of casting method, as shown in Fig. 4.2, which is horizontal casting and vertical casting were used. The testing parameter is the casting direction along the horizontal and vertical directions. Specimens are listed in Table. 4.1. Specimen No. 24 of which has been reported in the previous study [4.5] are also discussed. Specimen No.24 is the control sample in which there is no fiber in panel zone. Characteristics of PVA fiber are listed in Table 4.2. All specimens are designed to fail by shear in panel zone before flexural yielding as same as the specimens in Chapter 3. Mechanical properties of concrete and PVA FRCC are listed in Table 4.3.

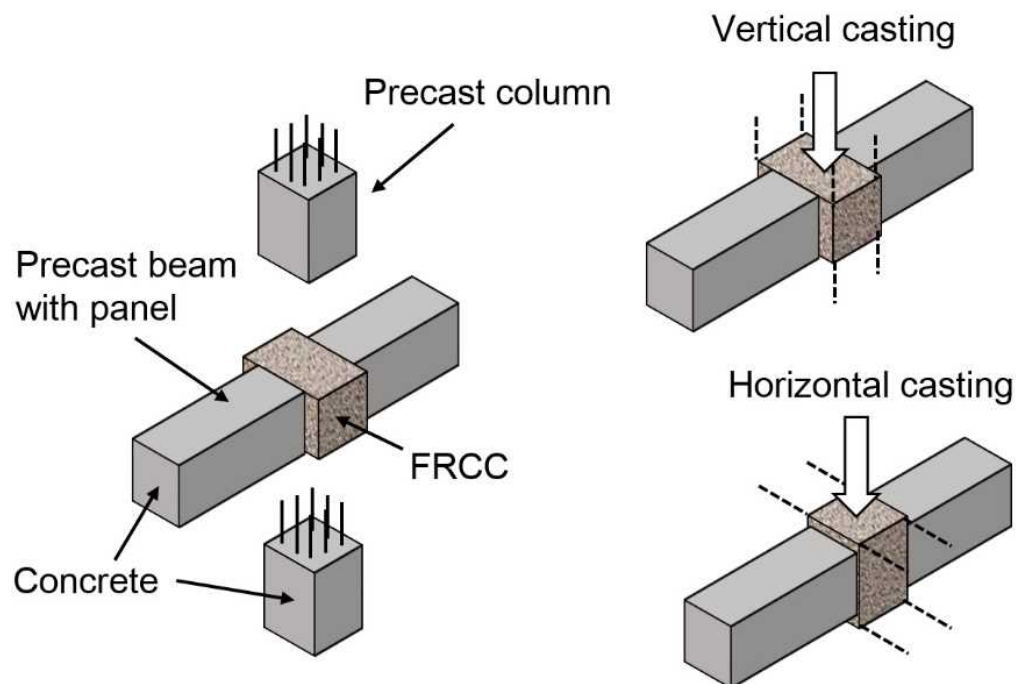


**Fig. 4. 2 Casting directions**

**Table 4. 1 Specimens list**

ID	Panel	Beam		Column	
	Parameter	Reinforcing bar	Stirrup	Reinforcing bar	Hoop
No.24*	Without fiber	18-D22 (USD685)	6-D10@60 (SD785)	16-D22 (USD685)	6-D10@60 (SD785)
No.32	Horizontal casting Vibrator				
No.33	Vertical casting Vibrator				

\*Specimen No.24 is from the previous study (Sano et al., 2015) [4.5]

**Table 4. 2 Mechanical properties of fiber**

Fiber	Length (mm)	Diameter (mm)	Tensile strength (MPa)	Elastic modulus (GPa)
PVA	12.0	0.10	1200	28

**Table 4. 3 Mechanical properties of concrete and PVA FRCC**

Type	ID	Place	Compressive strength (MPa)	Splitting tensile strength (MPa)	Elastic modulus (GPa)
Concrete	No.24*	Beam Column	39.9	3.55	29.6
PVA FRCC	No.24*	Panel zone	50.3	-	17.6
Concrete	No.32	Beam	75.5	4.47	35.0
	No.33	Column	75.6	4.11	33.3
PVA FRCC	No.32	Panel	49.1	-	17.1
	No.33	zone	48.0	-	15.7

\*Specimens No.24 is from the previous study (Sano et al., 2015) [4.5]

#### 4.2.2 Casting methods

As shown in Fig. 4.3, horizontal casting is to cast FRCC from beam side into panel zone. Otherwise vertical casting is to cast FRCC from column side into panel zone which is shown in Fig. 4.4. During the casting, a vibrator rod was being inserted into the matrix along with the direction of casting to arrange the fiber orientation of panel zone. As shown in Fig. 4.5, first pour the FRCC into panel zone mold to half, second insert a vibrator rod for 45 seconds. Then continue to pour FRCC into panel zone mold to full and insert a vibrator rod for 45 seconds again. Other procedures of making specimens is as the same as described in Chapter 3.

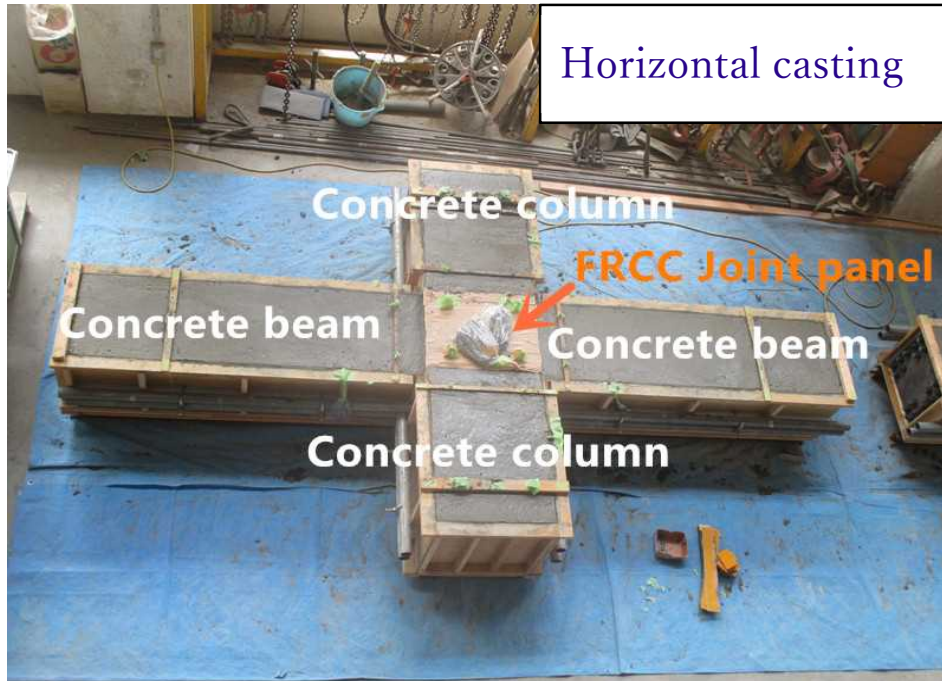


Fig. 4. 3 Example of horizontal casting

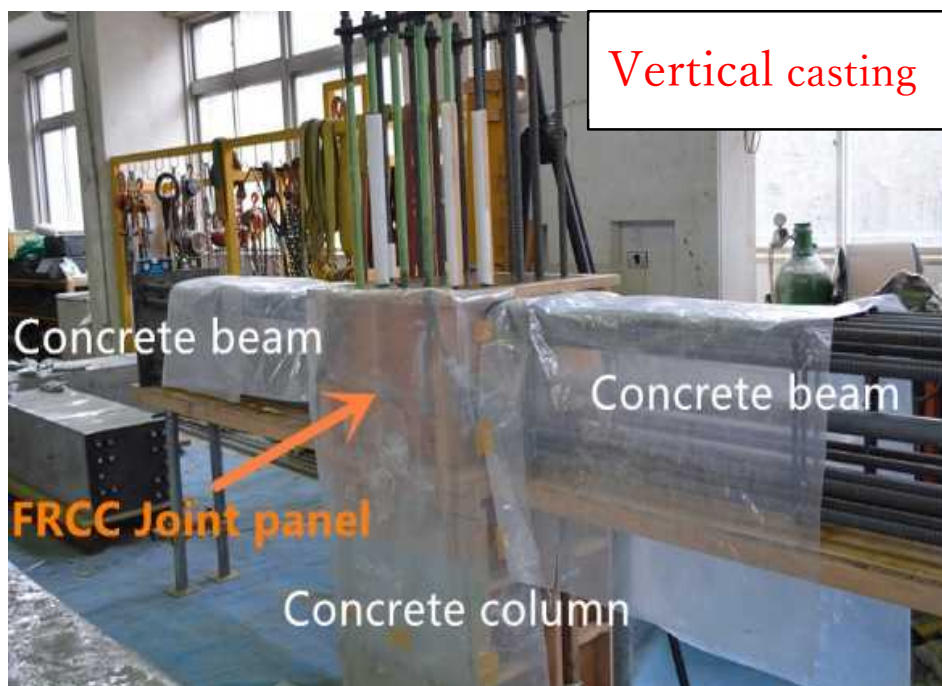
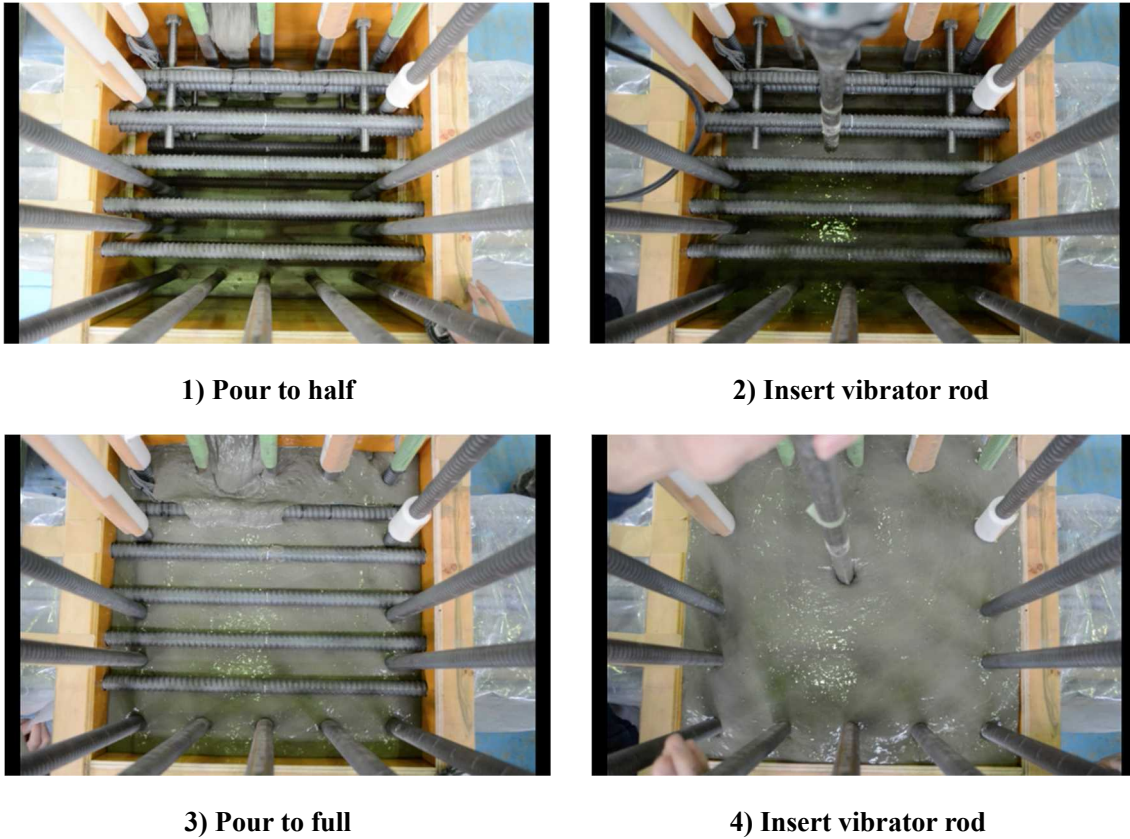


Fig. 4. 4 Example of vertical casting



**Fig. 4. 5 Casting procedures**

#### 4.2.3 Loading and measurement

As introduced in Chapter 3, the reversed cyclic loading is applied to the beams by controlling story drift angles from  $R = \pm 1/400$  to  $\pm 1/20$ rad. The story drift angle was controlled by actuators attached to the inflection points of the beams. Oil jacks were used on the inflection points to support the columns.

#### 4.2.4 Experimental results

##### 4.2.4.1 Failure modes and crack patterns

The crack patterns of panel zone at maximum load are shown in Fig. 4.6. Shear cracks were observed on the surface of panel zone of both two specimens. The failure in strut mechanism of specimen No. 32 was observed at the story drift angle of  $1/50$ rad. From the next loading cycle, the shear sliding was observed. As mentioned in Chapter 3, specimen No.32 had a same tendency with specimen No. 25 of which the pull-out of fibers were observed obviously in the loading cycle of  $R = 1/50$ rad. As shown in Fig. 4.7, three penetrating cracks were occurred after the maximum load in the cover of specimen No. 33 along the middle main reinforcing bars direction. Red dot lines indicate the positions of the main reinforcing bars along the longitudinal direction of column.

The surface of No. 33 facing to the camera is also the side surface during vertical casting. Due to the existing of main bars, it is considered that fibers rarely distribute in this plane which leads to the reduction of fibers.



**Fig. 4. 6 Crack pattern at maximum load (No.32 at 1/50rad., No.33 at 1/67rad.)**

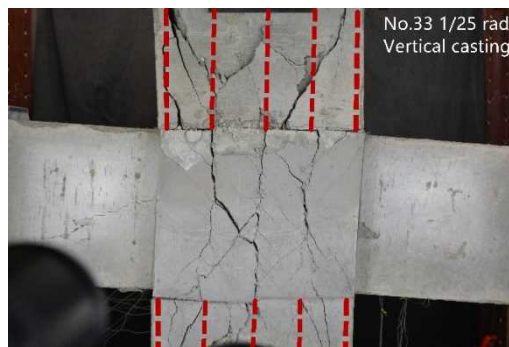


**Fig. 4. 7 Position of main reinforcing bars in column**

#### 4.2.4.2 Relationships of shear force and story drift angle

The relationship between the applied load on beams (average of both beams) and the story drift angle of specimen No. 32 and No. 33 are shown in Fig. 4.8. The maximum load of specimen No. 32 was observed at the cycle of 1/50 rad. and that of No. 33 was at 1/67 rad. After the maximum load, although the crack width increased with the increase of story drift angle, damage of joint panel was inhibited by the fiber bridging effect comparing to specimen No. 24. And also the maximum loads of beam-column joints increase by adding fiber. It can be recognized that part of the shear force was carried by PVA fibers. From the comparison between specimens No. 32 and No. 33, of which maximum load is 461 kN and 468 kN respectively. This indicates that casting direction of panel zone do not affect shear capacity of PVA FRCC beam-column joint significantly.

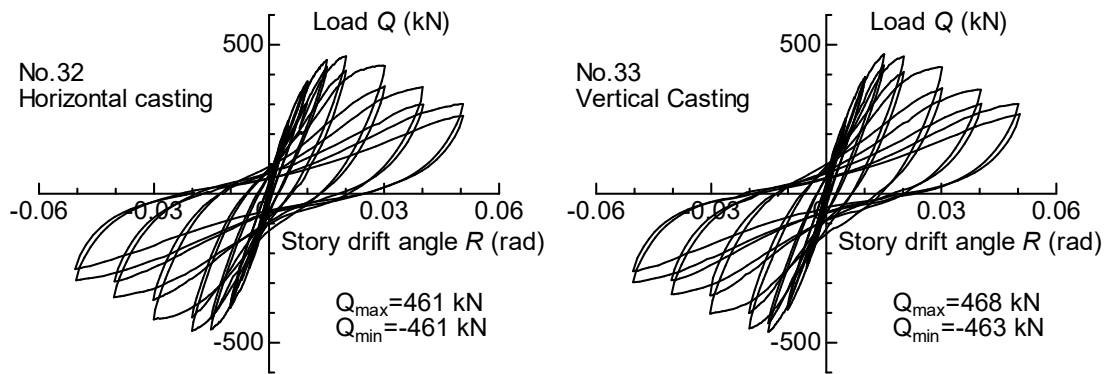


**Fig. 4. 8 Load-story drift angle curve**

#### 4.2.4.3 Comparison of skeleton curves

Skeleton curves of specimens No. 24\* (without fiber), No. 32 (horizontal casting + vibrator) and No. 33 (vertical casting + vibrator) are shown in Fig. 4.9. Compared with specimen No. 24, higher maximum load was observed in both No. 32 and No. 33. Specimens of horizontal casting and vertical casting showed almost the same shear capacities.

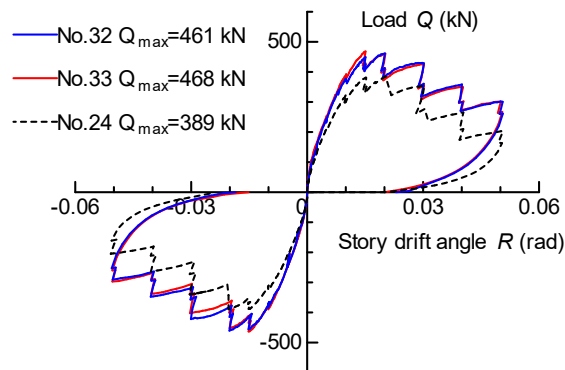


**Fig. 4. 9 Comparison of skeleton curves**

\*Specimen No.24 is from the previous study (Sano et al., 2015) [4.5]

#### 4.3 Conclusions

The maximum load of horizontal casting specimen was observed at the cycle of 1/50 rad. and that of vertical casting specimen was at 1/67 rad. After the maximum load, although the crack width increased with the increase of story drift angle, damage of joint panel was inhibited by the fiber bridging effect comparing to specimen without fiber. From the comparison between horizontal specimen and vertical specimen, of which maximum load is 461 kN and 468 kN respectively. This indicates that casting direction of panel zone do not affect shear capacity of PVA FRCC beam-column joint significantly. Specimens of horizontal casting and vertical casting show almost the same shear capacities.

## CHAPTER 5 Evaluation of Shear Capacity of FRCC Beam-Column

### Joints

#### 5.1 Introduction

By assuming that the shear stress in the panel zone is also carried by fiber bridging effect, shear capacity of beam-column joint is evaluated through the tensile characteristics of FRCC.

In the previous study, as mentioned in Chapter 3, the maximum load of beam-column joint specimen No. 24 (without fiber) occurred in the loading cycle of  $R = 1/50$ rad. and was keeping almost unchanged from loading of  $R = 1/67$ rad. to  $R = 1/33$ rad. [5.1]. It is considered that the compressive strut had achieved the effectiveness compressive capacity around  $R = 1/50$  rad. Meanwhile, the failure in strut mechanism of specimen No. 31 (PP) and specimen No. 32 (PVA) was observed at story drift angle of  $R = 1/50$ rad. In the case of specimen No. 30 (aramid), the compressive strut crushed at story drift angle of  $R = 1/33$  rad.

For the No. 31 (PP) and specimen No. 32 (PVA), the strut mechanism was remained to the loading cycle of  $R = 1/67$  rad. due to the fiber bridging effect. From the next loading cycle, the shear sliding was observed obviously. It is considered that the pull-out of fibers became prominent which resulted in the maximum load under biaxial stress condition. The same tendency was also observed in the case of specimen No. 30 (aramid). The pull-out of fibers were observed obviously in the loading cycle of  $R = 1/33$ rad. which led to the maximum load.

At the maximum load, by assuming failure of strut mechanism and disappear of fiber bridging effect are occurred simultaneously [5.2], a cumulative sum calculation method is newly proposed to predict the shear capacity of FRCC beam-column joint based on AIJ guideline [5.3].

#### 5.2 Proposed Evaluation Method for FRCC Beam-Column Joint

A shear capacity predicting method has been proposed for conventional concrete beam-column joint by AIJ guideline [5.3]. The main idea is to treat shear force of panel zone as the difference between beam shear force and column shear force. According to the Design Guidelines for Earthquake Resistant Reinforced Concrete Buildings Based on Inelastic Displacement Concept of AIJ guideline, the shear capacity carried by concrete is given by Eq. (5.1).

$$V_{jc} = \kappa \cdot \varphi \cdot F_j \cdot b_j \cdot D_j \quad (5.1).$$

where  $V_{jc}$  is shear capacity by AIJ guideline;  $\kappa$  is shape coefficient;  $\varphi$  is orthogonal beam coefficient;  $F_j$  is shear strength of panel zone;  $b_j$  is effective width;  $D_j$  is column height;

In a FRCC beam-column joint, the fiber bridging effect is mainly distributed in the direction which is perpendicular the diagonal shear crack. After cracking, fibers could transfer tensile force through crack as shown in Fig. 5.1

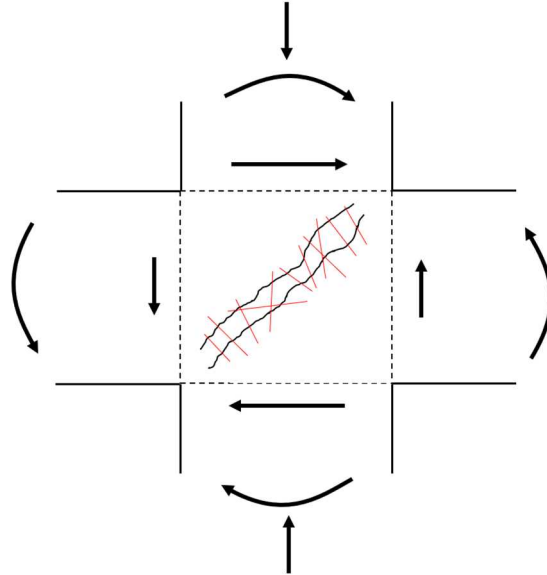


**Fig. 5. 1 Internal actions into panel zone**

As shown in Fig. 5.2, the total tensile force carried by fibers at maximum load can be calculated by the maximum tensile stress which was obtained from the uniaxial tension test as given by Eq. (5.2). The crack angle  $\theta$  is observed directly from the surface of panel zone. The second peak loads in uniaxial tension test with notched specimens are adopted for maximum tensile stress in each type of fibers. The effective depth of 346 mm was adopted for this calculation.

$$N = \sigma_{t,\max} \cdot \frac{d_b}{\sin \theta} \cdot b_j \quad (5.2)$$

where  $N$  is the tensile force;  $\sigma_{t,\max}$  is maximum FRCC tensile stress;  $d_b$  is effective depth of beam;  $\theta$  is the crack angle;  $b_j$  is effective width.

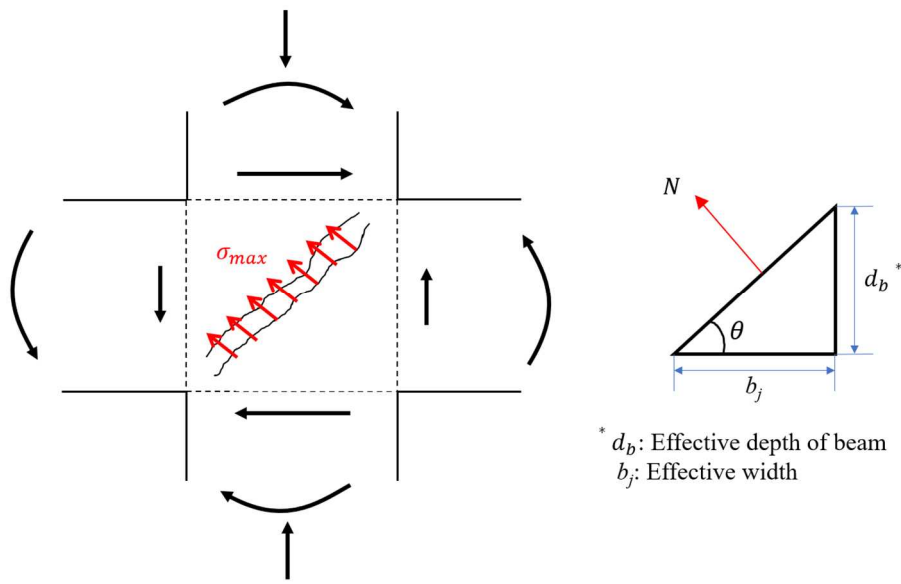


**Fig. 5. 2 Calculation of tensile force**

As shown in Fig. 5.3, shear force is derived from tension force carried by fibers as given by Eq (5.3). The parameters used for calculation are listed in Table 5.1.

$$\begin{aligned}
 V_{ff} &= N \cdot \sin \theta \\
 &= \sigma_{t,\max} \cdot d_b \cdot b_j
 \end{aligned}
 \tag{5.3}$$

where  $V_{ff}$  is shear capacity carried by fiber;  $N$  is the tensile force;  $\theta$  is the crack angle;  $\sigma_{t,\max}$  is maximum FRCC tensile stress;  $d_b$  is effective depth of beam;  $b_j$  is effective width.

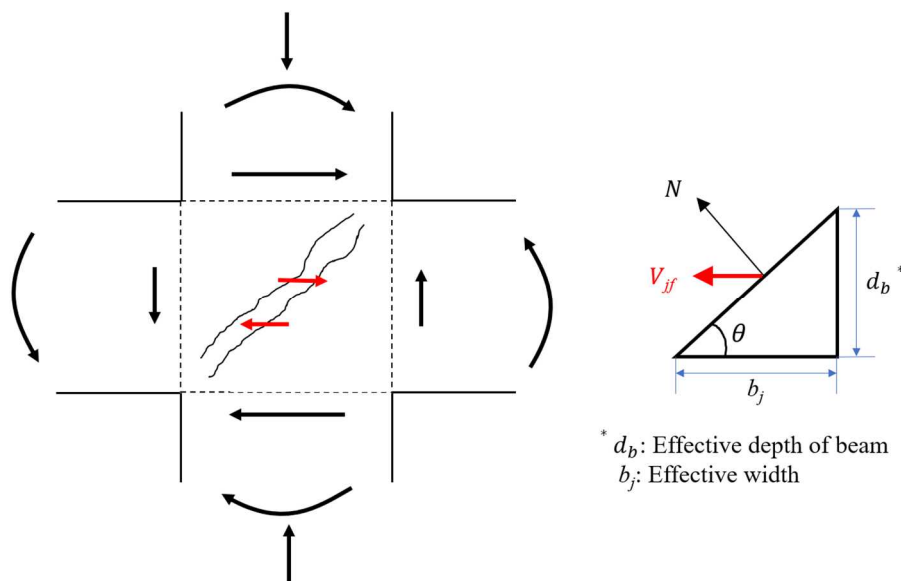


**Fig. 5. 3 Calculation of shear force**

**Table 5. 1 Parameters for tensile force calculation**

ID	Used fiber	Maximum	Effective	Effective
		tensile stress	depth of beam	width
		$\sigma_{t,max}$ (MPa)	$d_b$ (mm)	$b_j$ (mm)
No. 30	Aramid	3.02	346	440
No. 31	PP	1.61		
No. 32	PVA	1.80		

At the maximum load, by assuming failure of strut mechanism and disappear of fiber bridging effect are occurred simultaneously, calculation method for shear capacity of FRCC beam-column joint Eq. (5.4) can be proposed. Eq. (5.4) is derived as the summation of the Eq. (5.1) given by Design Guidelines for Earthquake Resistant Reinforced Concrete Buildings Based on Inelastic Displacement Concept [5.3] to shear force carried by FRCC expressed by Eq. (5.3).

$$V_{ju} = V_{jc} + V_{jf} \quad (5.4)$$

where  $V_{ju}$  is shear capacity;  $V_{jc}$  is shear capacity by AIJ guideline;  $V_{jf}$  is shear capacity carried by fiber.

### 5.3 Verification

Experimental and calculated values of shear capacities are converted to the shear force which is applied to beam. As listed in Table 5.2, the difference of below 7% between calculated value and experimental value demonstrates that the calculation method is feasible. By adopting this method, shear capacity of FRCC beam-column joint can be calculated from the result of uniaxial tension test.

**Table 5. 2 Experimental value and calculated value**

		No fiber (No. 24)	Aramid (No. 30)	PP (No. 31)	PVA (No. 32)
Experimental value $V_{exp}$ (kN)		389	544	495	461
Calculated value	Eq. (5.1) $V_{jc}$ (kN)	419	424	426	412
	Eq. (5.3) $V_{jf}$ (kN)	0	83	44	49
	Eq. (5.4) $V_{ju}$ (kN)	419	507	470	461
$V_{exp} / V_{ju}$		0.93	1.07	1.05	1.00

#### 5.4 Conclusions

A cumulative sum calculation method is newly proposed to predict the shear capacity of FRCC beam-column joint based on AIJ guideline. By adopting maximum tensile stress obtained from uniaxial tension test of specimen with notch, shear force carried by fibers was calculated. The difference of below 7% between calculated value and experimental value demonstrates that the calculation method is feasible. By adopting this method, shear capacity of FRCC beam-column joint can be calculated from uniaxial tension test.

## Chapter 6 Conclusions

FRCC as a new material was successfully used in the beam-column joint to strengthen the crucial part of a RC structure. Beam-column joint test of specimens using aramid, PP and PVA fiber as volume fraction of 1% was conducted to seek the influence of fiber types on the shear performance of FRCC beam-column joint. Furthermore, The influence of casting direction on the shear performance of FRCC beam-column joint was discussed through two specimens using PVA fiber as volume fraction of 1% which were manufactured by horizontal casting and vertical casting. In addition, tensile and flexural behavior of FRCC obtained by uniaxial tension test and bending test could be used to evaluate the shear capacity of FRCC beam-column joint. A new calculation method for predicting the shear capacity of FRCC beam-column joint based on AIJ guideline has been proposed. The main conclusions of this research are summarized as below.

1. The average maximum tensile stress of Aramid specimen with notch at second peak is 3.02MPa, of that for PP specimen is 1.61MPa and PVA specimen 1.80 MPa which could be used to evaluate the structural performance of FRCC.
2. Comparing with specimen without fiber, the damage of beam-column joint with fibers is inhibited due to the effect of fiber bridging.
3. Specimen No.30 has the highest maximum load which is 544kN. It is recognized that the bridging effect is different by types of fiber.
4. Specimens of horizontal casting and vertical casting show almost the same shear capacities.
5. A new calculation method for evaluating shear capacity of FRCCs beam-column joint is proposed based on the standard of Architectural Institute of Japan. The difference of below 7% between calculated value and experimental value demonstrates that the calculation method is feasible.

The following recommendations for future study are introduced.

1. Large-diameter fibers were adopted in this research. With the development of polymer fibers, many small-diameter fibers have been studied recent years. Compared to large-diameter fibers, small-diameter fibers have a better bond strength due to the larger aspect ratio. It is expected that small-diameter fibers could be used in real RC structures. However, the structural performance of materials with small-diameter fibers still remain too many unknown, more researches should be conducted.

2. The shear force was treated as component of tensile force in this research. However, in the case of beam-column joint under shear, the biaxial stress condition is very complicated. Direct shear test is required to investigate the shear transmission on the crack surface under the tensile action.

3. Further experimental studies over a variety of parameters, such as different fiber volume fraction, should be conducted in the future study.

## REFERENCES

### CHAPTER 1

- [1.1] Hannant, D. J., "Fibre Cements and Fiber Concretes" 219 PP., ISBN 0 471 99620 3, Published 1978.
- [1.2] Ashik, K. P., and Sharma, R. S., "A Review on Mechanical Properties of Natural Fiber Reinforced Hybrid Polymer Composites," *Journal of Minerals and Materials Characterization and Engineering*, 2015, 3, pp.420-426.
- [1.3] Ramakrishna, G., and Sundararajan, T., "Studies on the durability of natural fibres and the effect of corroded fibres on the strength of motar," *Cem. Concr. Cpmpos.* 27(2005) pp.575-582.
- [1.4] Reddy, N., and Yang, Y., "Biofibers from agricultural byproducts for industrial applications" *Trends Biotechnol.* 23(1) (2005) pp.22-27.
- [1.5] Arsene, M. A., Jr. Savastano, H., Allameh, S.M., Ghavami, K., and Soboyejo, W., "Cementitious composites reinforced with vegetable fibers, " *Proceedings of the First Inter-American Conference on Non-conventional Materials and Technologies in the Eco-construction and Infrastructure*, Joao-Pessoa, Brazil, November 2003, pp. 13-16.
- [1.6] Onuaguluchi, O., and Banthia, N., "Plant-based natural fibre reinforced cement composites: A Review," *Cement and Concrete Composites* 68(2016) pp.96-108
- [1.7] Li, V. C., "Large volume high performance applications offibers in civil engineering, " *J. Appl. Polym. Sci.* 83 (2002) pp.660–686
- [1.8] Prisco, M. D., and Plizzari, G. A, "Precast SFRC elements: From Material Properties to Structural Applications," 6th RILEM Symp. Fibre-Reinforced Concr.- BEFIB 2004, Varenna, Italy, pp.81-100.
- [1.9] Serna, P., Arango, S.,Ribeiro, T., Núñez, A. M., and Taengua, E. G., "Structural cast-in-place SFRC: technology, control criteria and recent applications in spain," *Mater. Struct.* 42 (2009) pp.1233–1246.
- [1.10] G.A. Plizzari, G. Tiberti, "Steel fibers as reinforcement for precast tunnel segments," *Tunn. Undergr. Sp. Technol.* 21 (2006) pp.438–439.
- [1.11] Rivaz, B. E., "Durability issue for SFRC precast segment in tunneling application," WUTC2010, World Urban Transit Conference, Sentosa, Singapore, 2010, pp. 1–10.
- [1.12] G.T. Halvorsen, C.E. Kesler, A.R. Robinson and J.A. Stout, "Durability and Physical Properties of Steel Fiber Reinforced Concrete, " Illinois, US, Illinois, US (1976).
- [1.13] R. Winterberg, "Performance and durability improvements of precast concrete lining segments with fibre reinforcement, " *Australasian Institute of Mining and Metallurgy (Ed.)*, 14th Australas. Tunn. Conf. 2011 Dev. Undergr. Space, Proc, Australasian Institute of Mining and

Metallurgy, Auckland, New Zealand (2011), pp. 645-656.

[1.14] E.S. Bernard, "Durability of cracked fibre reinforced shotcrete," Shotcrete More Eng. Dev. Proc. Second Int. Conf. Eng. Dev. Shotcrete, A.A. Balkema Publishers, Sydney, Australia (2004), pp. 59-66.

[1.15] Meson., V. M., Michel, A., Solgaard, A., and Fischer, G., "Corrosion resistance of steel fibre reinforced concrete - A literature review," Cement and Concrete Research 103 · October 2017 PP.1-20.

[1.16] ACI Committee 544. 1R-96, State of the Art Report on Fiber Reinforced Concrete, pp. 39-57, 1996

[1.17] Li, V. C., "Engineered Cementitious Composites—Tailored Composites through Micromechanical Modeling," Fiber-Reinforced Concrete: Present and the Future, N. Banthia, A. Bentur, and A. Mufri, eds., Canadian Society for Civil Engineering, Montreal, Canada, 1998, pp. 64-97.

[1.18] Stang, H., and Li, V. C., "Extrusion of ECC Material," Proceedings of the 3rd RILEM/ACI Workshop: High-Performance Fiber-Reinforced Cement Composites, H. W. Reinhardt and A. E. Naaman, eds., E&FN Spon, London, 1999, pp. 203-212.

[1.19] Li, V. C., Wang S., and Wu C., "Tensile Strain-Hardening Behavior of Polyvinyl Alcohol Engineered Cementitious Composite (PVA-ECC)," ACI Materials Journal, Technical Paper, Tile no. 98-M52, Volume: 98 Issue: 6, 11/1/2001pp.483-492.

[1.20] Architectural Institute of Japan, "Design Guidelines for Earthquake Resistant Reinforced Concrete Buildings Based on Ultimate Strength Concept," 1990

[1.21] Fujiu, N., and Sugimoto, K., "Development of Precast System for Constructuon High-rise RC Buildings in Short Term," Concrete Journal, Vol.47, No.8 pp.25-32. Aug, 2009 (*in Japanese*)

[1.22] Henager, C. H., "Steel Fibrous Ductile Concrete Joint for Seismic- Resistant Structures," Reinforced Concrete Structures in Seismic Zones, SP-53, American Concrete Institute, Detroit, 1977, pp. 371-386.

[1.23] Halvorsen, G. T., and Kesler, C. E., "Moment-Curvature Relationships for Concrete Beams with Plain and Deformed Steel Fibers," ACI JOURNAL Proceedings V. 76, No. 6, June 1979, pp. 697-706.

[1.24] Craig, R.; Mahadev, S.; Patel, C. C.; Viteri, M.; and Kertesz, C., "Behavior of Joints Using Reinforced Fibrous Concrete," Fiber Reinforced Concrete—International Symposium, SP-81, American Concrete Institute, Detroit, 1984, pp. 125-167.

[1.25] Naaman, A. E.; Wight, J. K.; and Abdou, H., "SIFCON Connections for Seismic Resistant Frames," Concrete International: Design & Con- struction, V. 9, No. 11, Nov. 1987, pp. 34-39.

- [1.26] Gefken, P. R., and Ramey, M. R., "Increased Joint Hoop Spacing in Type 2 Seismic Joints Using Fiber Reinforced Concrete," *ACI Structural Journal*, V. 86, No. 2, Mar.-Apr. 1989, pp. 168-172.
- [1.27] Jiuru, T.; Chaobin, H.; Kaijian, Y.; and Yongcheng, Y., "Seismic Behavior and Shear Strength of Frames Joint Using Steel-Fiber Reinforced Concrete," *Journal of Structural Engineering*, ASCE, V. 118, No. 2, Feb. 1992, pp. 341-358.
- [1.28] Durrani, A. J., and Diaz, A. J., "Seismic Resistance of Fiber-Reinforced Slab-Column Connections," *Tenth World Conference on Earthquake Engineering*, Madrid, July 1992, pp. 3113-3116.
- [1.29] Filiatrault, A., Pineau, S., and Houde, J., "Seismic Behavior of Steel-Fiber Reinforced Concrete Interior Beam-Column Joints," *ACI Structural Journal*, V. 92, No. 5, Nov. 1995, pp. 543-552.
- [1.30] Kosa, K, and Naaman, A. E., "Corrosion of Steel Fiber Reinforced Concrete," *ACI Materials Journal*, V. 87, No. 1, Jan.-Feb. 1990, pp. 27-37.
- [1.31] Kosa, K, Naaman, A. E., and Hanse, W., "Durability of Fiber Reinforced Mortar," *ACI Materials Journal*, V. 88, No. 3, May 1991, pp. 310-319.
- [1.32] Mu, Y., and Kanakubo, T., "Bending Test of FRC Notched Beam with Various Polymer Fibers," *Summaries of technical papers of annual meeting Architectural Institute of Japan (TOHKAI), material construction*, pp.511~512, 2015.9
- [1.33] Kanakubo, T., Miyaguchi, M., and Asano, K., "Influence of Fiber Orientation on Bridging Performance of Polyvinyl Alcohol Fiber-Reinforced Cementitious Composite." *Materials Journal*, American Concrete Institute, Vol.113, No.2, Mar. 2016, pp.131-141.
- [1.34] Sano, N., Yamada. H., Miyaguchi, M., Yasojima, A., and Kanakubo, T., "Structural Performance of Beam-Column Joint using DFRCC, " *11th Canadian Conference on Earthquake Engineering -Facing Seismic Risk-*, Paper ID 94163, 2015.7
- [1.35] Yamada, H., Ando, M., Yasojima, A., and Kanakubo, T., "Effect of Fiber Types on Shear Performance of Precast Concrete Beam-Column Joints Using DFRCC", *ACF 2016, The 7th International Conference of Asian Concrete Federation*, 3. Concrete structures, Paper No.46, 2016.10
- [1.36] Zhang, R., Matsumoto, K., Hirata, Ishizeki, Y., and Niwa, J., "Application of PP-ECC in beam-column joint connections of rigid-framed railway bridges to reduce transverse reinforcements," *Engineering Structures*, V. 86, Mar. 2015, pp. 146-456.
- [1.37] Architectural Institute of Japan, "Design Guidelines for Earthquake Resistant Reinforced Concrete Buildings Based on Inelastic Displacement Concept," 1999

## CHAPTER 2

- [2.1] Kansai, Y. and Ikeda, N. eds, "Testing Method of Concrete, 1993," 2<sup>nd</sup> Volume. Tokyo: Gijutsu Shoin. (in Japanese).
- [2.2] Akitam H., Koide, H., and Mihashi, H., "Experimental validation in the effect of secondary flexure in uniaxial tension of concrete," Proceedings CD-ROM of 11<sup>th</sup> International Conference on Fracture, Paper No.5573, 2005
- [2.3] Kanakubo, T., "Tensile Characteristics Evaluation Method for Ductile Fiber-Reinforced Cementitious Composites, " Journal of Advanced Concrete Technology, Vol.4, No.1, pp.3-17, 2006.2
- [2.4] Kanakubo, T., Miyaguchi, M., and Asano, K., "Influence of Fiber Orientation on Bridging Performance of Polyvinyl Alcohol Fiber-Reinforced Cementitious Composite, " Materials Journal, American Concrete Institute, Vol.113, No.2, pp.131-141, 2016.3
- [2.5] Kanda, T.; Tomoe, S.; Nagai, S.; Maruta, M.; Kanakubo, T.; and Shimizu, K., "Full Scale Processing Investigation for ECC Pre-Cast Structural Element," Journal of Asian Architecture and Building Engineering, V. 5, No. 2, 2006, pp. 333-340. doi: 10.3130/jaabe.5.333
- [2.6] Japan Society of Civil Engineers, "Standard Specifications for Concrete Structures — 2013, Test Methods and Specifications," JSCE Standard, 2013, 2013, pp. 281-282. (in Japanese)
- [2.7] Sano, N., Yamada. H., Miyaguchi, M., Yasojima, A., and Kanakubo, T., "Structural Performance of Beam-Column Joint using DFRCC, " 11th Canadian Conference on Earthquake Engineering -Facing Seismic Risk-, Paper ID 94163, 2015.7
- [2.8] Japan Concrete Institute, "Method of Test for Load-displacement Curve of Fiber Reinforced Concrete by Use of Notched Beam, " JCI-S-002-2003
- [2.9] Japan Concrete Institute, "Method of Test for Bending Moment – Curvature Curve of Fiber Reinforced Cementitious Composites, " JCI-S-003-2007

## CHAPTER 3

- [3.1] Fujiu, N., and Sugimoto, K., "Development of Precast System for Constructuon High-rise RC Buildings in Short Term, " Concrete Journal, Vol.47, No.8 pp.25-32. Aug, 2009
- [3.2] Sano, N., Yamada. H., Miyaguchi, M., Yasojima, A., and Kanakubo, T., "Structural Performance of Beam-Column Joint using DFRCC, " 11th Canadian Conference on Earthquake Engineering -Facing Seismic Risk-, Paper ID 94163, 2015.7

#### CHAPTER 4

- [4.1] Laranjeira, F.; Aguado, A.; Molins, C.; Grünewald, S.; Walraven, J.; and Cavalaro, S., “Framework to Predict the Orientation of Fibers in FRC: A Novel Philosophy,” *Cement and Concrete Research*, V. 42, No. 6, 2012, pp. 752-768. doi: 10.1016/j.cemconres.2012.02.013
- [4.2] Kanakubo, T., Miyaguchi, M., and Asano, K., “Influence of Fiber Orientation on Bridging Performance of Polyvinyl Alcohol Fiber-Reinforced Cementitious Composite, ” *Materials Journal*, American Concrete Institute, Vol.113, No.2, pp.131-141, 2016.3
- [4.3] Watanabe, K., Ozu, Y., Miyaguchi, M., and Kanakubo, T., Influence of Placing Method Considering Fiber Orientation to Bending Characteristics of DFRCC, ACF 2016, The 7th International Conference of Asian Concrete Federation, 1. Concrete materials and technologies, Paper No.43, 2016.10
- [4.4] Watanabe, K., Ozu, Y., Kanakubo, T., “Visualization Simulation of Fiber Orientation in DFRCC Members by Fiber-Controlling Pouring Method”, Summaries of technical papers of annual meeting Architectural Institute of Japan (Kyusyu), material construction, pp.461-462, 2016. (*in Japanese*)
- [4.5] Sano, N., Yamada. H., Miyaguchi, M., Yasojima, A., and Kanakubo, T., “Structural Performance of Beam-Column Joint using DFRCC, ” 11th Canadian Conference on Earthquake Engineering -Facing Seismic Risk-, Paper ID 94163, 2015.7

#### CHAPTER 5

- [5.1] Sano, N., Yamada. H., Miyaguchi, M., Yasojima, A., and Kanakubo, T., “Structural Performance of Beam-Column Joint using DFRCC, ” 11th Canadian Conference on Earthquake Engineering -Facing Seismic Risk-, Paper ID 94163, 2015.7
- [5.2] Yasojima, A., Yamada, H., Ozu, Y., and Kanakubo, T., “Evaluation of Shear Capacity of SFRCC PCa Beam-Column Joint Based on Shear Bridging Characteristics of Fibers,” *Proceedings of the Japan Concrete Institute*, Vol.40, No.2, pp.1201-1206, 2018.7 (*in Japanese*)
- [5.3] Architectural Institute of Japan, “Design Guidelines for Earthquake Resistant Reinforced Concrete Buildings Based on Inelastic Displacement Concept,” 1999

## **ACKNOWLEDGEMENTS**

Please allow me to express my sincerest appreciation to my academic supervisor, Professor Toshiyuki Kanakubo, for his precious guidance, constructive supervision, priceless feedback, and pleasant communication during this research project. Without his advice and guidance, this thesis could not be completed. Without his encouragement and support, I could not finish my study. His extensive research experience and keen insight have impressed me deeply and will certainly encourage me for the rest of my life.

I would like to thank my vice-academic supervisor Associate Professor Akira Yasojima and a technical staff member Mr. Kojima, for their extremely important assistance on my experiment and their valuable comments on my research.

I would also like to acknowledge my thesis committee members, Prof. Sakai, Prof. Matsushima, and Dr Suwada, for their valuable advices and constructive instructions.

I would also want to thank Mr. Naoya Sano, Mr. Hiroshi Yamada and Mr. Faizal Hanif, for their assistance of contribution on my research work.

I also thank all the students in this laboratory. I have learned a lot from them.

At last, special thanks are also expressed to my dearest parents for their endless love and continuous support.

## PUBLICATIONS ARISING FROM THE THESIS

1. **Yu Mu** and Toshiyuki Kanakubo:

“Bending Test of FRC Notched Beam with Various Polymer Fibers”, Summaries of Technical Papers of Annual Meeting, Architectural Institute of Japan, Materials and Construction, pp.511-512, 2015.9

2. **Yu Mu** and Toshiyuki Kanakubo:

“Influence of Notch on Bending and Tensile Characteristics of FRCC”, Summaries of Technical Papers of Annual Meeting, Architectural Institute of Japan, Materials and Construction, pp.171-172, 2017.8

3. **Yu Mu**, Mai Ando, Akira Yasojima, and Toshiyuki Kanakubo:

“Influence of Fiber Orientation on Structural Performance of Beam-Column Joints Using PVA FRCC”, Strain-Hardening Cement-Based Composites, SHCC4, RILEM Bookseries 15, pp.465-472, 2017.9

4. Hiroko Hashimoto, **Yu Mu**, Hiroshi Yamada and Toshiyuki Kanakubo:

“Slip-Out Characteristics of Aramid and PP Fibers and Calculation of Bridging Law”, Concrete Research and Technology, Vol 28, pp. 103-111, 2017.11 (In Japanese)

5. **Yu Mu**, Arika Yasojima and Toshiyuki Kanakubo:

“Shear Performance of FRCC Beam-Column Joints Using Various Polymer Fibers”, Journal of Civil Engineering and Architecture, Volume 13, Number 9, pp.562-571, 2019.9